September 3, 2014

Multinuclear Solid-State NMR Studies of Polymer-Supported Scandium Triflate Catalysts

Aaron J. Rossini, *University of Windsor*
Marcel P. Hildebrand, *University of Windsor*
Paul A. Hazendonk, *University of Lethbridge*
Robert W. Schurko, *University of Windsor*

Multinuclear Solid-State NMR Studies of Polymer-Supported Scandium Triflate Catalysts

Aaron J. Rossini,[†] Marcel P. Hildebrand,[†] Paul A. Hazendonk,[‡] and Robert W. Schurko*[,†]

[†]Department of Chemistry and Biochemistry, University of Windsor, Windsor, Ontario N9B 3P4, Canada
[‡]Department of Chemistry and Biochemistry, University of Lethbridge, Lethbridge, Alberta T1K 3M4, Canada

S Supporting Information

ABSTRACT: Scandium(III) trifluoromethanesulfonate [Sc-(OTf)$_3$] is extensively used in organic synthesis to catalyze a wide variety of carbon–carbon bond-forming reactions in aqueous media. It has previously been demonstrated that it is possible to immobilize Sc(OTf)$_3$ in polystyrene (PS) to form the heterogeneous catalysts, microencapsulated (ME) Sc(OTf)$_3$. The ME catalysts are recoverable, reusable, often reduce metal leaching, and have activity similar to that of their homogeneous counterparts. Aside from preliminary scanning electron micros-copy (SEM) and energy dispersive X-ray (EDX) imaging studies and solution ^{45}Sc NMR studies, there is little information available about the molecular and bulk structure of the ME catalyst. In this regard, we have conducted a ^{45}Sc solid-state NMR investigation of the Sc environments in the crystalline and ME forms of anhydrous Sc(OTf)$_3$ and hydrated Sc(OTf)$_3$·8H$_2$O. Additional solid-state ^{1}H, ^{19}F, and ^{13}C NMR and powder X-ray diffraction experiments provide information that is complementary to that obtained from the ^{45}Sc NMR spectra, allowing for structural models of ME complexes to be proposed. The principal findings are that Sc(OTf)$_3$ is hydrated upon microencapsulation to form Sc(OTf)$_3$·8H$_2$O. ^{1}H–^{45}Sc TRAPDOR and ^{1}H–^{19}F CP SSNMR experiments and powder X-ray diffraction experiments suggest that Sc is dispersed throughout the polymer within nanocrystalline domains of Sc(OTf)$_3$·8H$_2$O. The approach outlined here should be applicable for the characterization of many other polymer-supported metal-based catalysts.
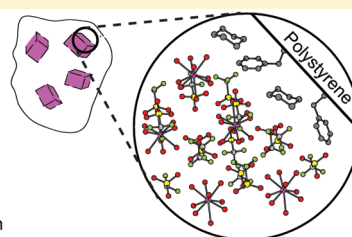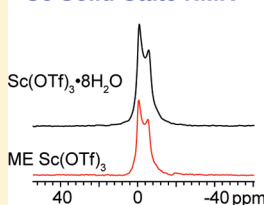
INTRODUCTION

Green chemistry is a term used to describe the creation of products or processes in chemistry that will reduce or eliminate hazardous byproducts or solvents.[1−4] One of the simplest ways to develop more environmentally friendly chemical processes is to eliminate potentially toxic and expensive organic solvents and stoichiometric reagents, and replace them with aqueous media and/or catalytic reagents.[5−7] There has been intense research in both academic and industrial sectors in developing water-tolerant reagents and catalysts.[7]

Kobayashi and co-workers have introduced scandium(III) trifluoromethanesulfonate (triflate) [Sc(OTf)$_3$] as an effective carbon–carbon bond-forming Lewis acid catalyst capable of catalyzing a variety of carbon–carbon bond-forming reactions in aqueous media.[8−19] This work is part of a larger field of research into water-tolerant Lewis acid catalysts.[7,20−22] In 1998, Kobayashi and co-workers introduced microencapsulation as a method of immobilizing Sc(OTf)$_3$ in polystyrene (PS).[23] These microencapsulated (ME) catalysts are recoverable, reusable, often reduce metal leaching, and have activities similar to those of their homogeneous counterparts; however, they are most often employed with organic solvents.[22] ME Sc(OTf)$_3$ has been shown to catalyze many of the same synthetic reactions as dissolved Sc(OTf)$_3$, while imparting the aforementioned beneficial characteristics of ME catalysts.[22,24,25] In some cases, ME Sc(OTf)$_3$ exhibits catalytic activity superior to that of

Sc(OTf)$_3$: for example, Lewis acids can be decomposed by basic aldimines; however, it was shown that ME Sc(OTf)$_3$ is able to tolerate and activate such aldimines without any notable decomposition.[22] In addition, ME Sc(OTf)$_3$ is able to catalyze Friedel–Crafts alkylation and acylation reactions,[26] which are important in large-scale reactions that exhibit characteristics desirable for green chemistry.[27−29]

Despite the importance of ME Sc(OTf)$_3$, the interactions between the microencapsulating polymer and Sc(OTf)$_3$ are not well understood. Kobayashi and co-workers characterized ME Sc(OTf)$_3$ by ^{45}Sc solution NMR spectroscopy[30] and energy dispersive X-ray (EDX) and scanning electron microscopy (SEM) imaging (in addition to reactivity studies).[23] EDX and SEM images showed that the Sc is well dispersed on the surface of the polymer in submicrometer size domains, which suggests the presence of nanocrystalline or molecular-level Sc(OTf)$_3$ domains in ME Sc(OTf)$_3$.[23] Solution ^{45}Sc NMR studies of acetonitrile solutions of ME Sc(OTf)$_3$ and Sc(OTf)$_3$ revealed a positive chemical shift difference of ca. +18 ppm for the former with respect to the latter, which is indicative of a major structural difference at the molecular level.[30] ^{45}Sc NMR of acetonitrile solutions of Sc(OTf)$_3$ with an added molecular PS

"analogue" (1,3,5-triphenylpentane) also displayed a positive chemical shift of ca. +14 ppm with respect to solutions Sc(OTf)$_3$.[30] Furthermore, the Sc loading levels were reduced when non-aromatic polymers such as polybutadiene and polyethylene were used as support materials for ME Sc(OTf)$_3$. Loading levels corresponding to 43% and 0% of the amount of Sc loaded into PS ME Sc(OTf)$_3$ were obtained with polybutadiene and polyethylene as the support materials, respectively. The solution ^{45}Sc NMR results and the higher loading levels observed for PS ME Sc(OTf)$_3$ were attributed by Kobayashi and co-workers to an interaction between the π-electrons of the PS phenyl groups and vacant Sc d-orbitals.[22,30] It was posited that this electronic interaction is responsible, in part, for immobilizing Sc(OTf)$_3$ in the polymer, with the steric bulk of the polymer also playing a role (i.e., physical envelopment of Sc(OTf)$_3$ by bulky phenyl groups may play a role in microencapsulation).[23]

Solid-state NMR (SSNMR) is an ideal technique for probing the structures of noncrystalline materials, such as polymers,[31−33] and by extension, polymer-based ME catalysts. In addition to SSNMR experiments on common nuclides, such as ^{1}H, ^{13}C, and ^{19}F, it is also possible to utilize ^{45}Sc (I = 7/2, N.A. = 100%) SSNMR to probe the structure of ME Sc(OTf)$_3$. ^{45}Sc SSNMR has recently been employed to probe the structure of a variety of scandium-containing materials,[34−54] and the ^{45}Sc quadrupole tensors and chemical shifts have been found to be very sensitive to the structural differences in local Sc environments.

In our preliminary study of Sc(OTf)$_3$ and ME Sc(OTf)$_3$,[37] we observed a single ^{45}Sc powder pattern (site) in the ^{45}Sc SSNMR spectra of both ME Sc(OTf)$_3$ and Sc(OTf)$_3$. The δ_{iso} of ME Sc(OTf)$_3$ was observed to be ca. +30 ppm higher than that of crystalline Sc(OTf)$_3$ (similar to the positive chemical shift differences observed in Kobayashi's solution ^{45}Sc NMR studies). Otherwise, similar electric field gradient (EFG) tensor and anisotropic chemical shift (CS) tensor parameters were observed in both cases. These preliminary results were consistent with Kobayashi's hypothesis that electronic interactions between the π-electrons of the PS phenyl groups and Sc are partly responsible for microencapsulation.[22,30] However, questions still remain regarding the local Sc environments in ME Sc(OTf)$_3$. This is further exacerbated by the absence of any known single-crystal X-ray diffraction (SCXRD) structure for Sc(OTf)$_3$.

Hence, further intensive study of Sc(OTf)$_3$ and ME Sc(OTf)$_3$ is necessary to understand the mode (and perhaps mechanism) of microencapsulation, as well as the local catalyst structure. To this end, we have acquired ^{45}Sc SSNMR NMR spectra of a series of ME Sc(OTf)$_3$ samples, freshly prepared under a variety of different conditions, as well as crystalline Sc(OTf)$_3$·8H$_2$O and ME Sc(OTf)$_3$·8H$_2$O. ^{1}H−^{45}Sc TRAP-DOR NMR experiments were employed to probe for possible interactions between the polymer and Sc atoms. In addition, solid-state ^{13}C, ^{19}F, and ^{1}H NMR experiments, as well as powder X-ray diffraction (PXRD) experiments, were also performed to obtain complementary information on the bulk structures of the ME catalysts.

EXPERIMENTAL SECTION

Sample Preparation. Samples of scandium trifluoromethanesulfonate [Sc(OTf)$_3$] were purchased from Strem Chemicals, Inc. and Sigma-Aldrich Chemicals, Inc. Some of the commercial samples of anhydrous Sc(OTf)$_3$ were found to

be partially hydrated when received, as indicated by ^{45}Sc SS NMR and/or PXRD. Completely anhydrous Sc(OTf)$_3$ was obtained by drying the powdered sample under vacuum at 160 °C for 4 h. Sc(OTf)$_3$·8H$_2$O and Sc(OTf)$_3$·8D$_2$O were synthesized by dissolving anhydrous Sc(OTf)$_3$ in H$_2$O and D$_2$O, respectively, followed by drying under vacuum at elevated temperatures (80 °C). Polystyrene (PS) (M_W = 60 500 and 22 400) and fully deuterated PS (PS-d_8, M_W = 66 000, approximately 98% deuterated) were purchased from Polymer Source Inc. and used without further purification.

Scandium acetate (Sc(OAc)$_3$) was purchased from Strem Chemicals, Inc. and purified by adding Sc(OAc)$_3$ to a 5.0 M glacial acetic acid solution. The solvent was then removed by vacuum, and the resulting solid was collected and isolated under inert atmosphere.[55] The identity of the purified sample was confirmed by PXRD.

Synthesis of Microencapsulated (ME) Sc(OTf)$_3$. The synthesis of ME Sc(OTf)$_3$ was based upon a modified literature procedure.[23] All reagents were handled under an inert N$_2$ atmosphere (except where noted), and all reactions were carried out using Schlenk lines. All solvents were dried by overnight reactions with calcium hydride, followed by distillations, with the exception of acetonitrile, which was obtained from a solvent system. 0.250 g of PS was combined with approximately 6 mL of cyclohexane in a Schlenk flask. The mixture was heated to 40 °C, while stirring, to dissolve the PS. 0.050 g of Sc(OTf)$_3$ (or Sc(OTf)$_3$·8H$_2$O, where indicated) was weighed into a first Schlenk flask. The hot PS/cyclohexane mixture was then cannulated into a second Schlenk flask containing Sc(OTf)$_3$ and stirred for 1 h at 40 °C. The mixture was slowly cooled to 0 °C in an ice bath, during which time PS was observed to precipitate. Eight milliliters of hexanes was then added in a dropwise manner to precipitate the remaining PS. After this, the solution was stirred at room temperature for 1 h. The solvent was pumped off, and the PS was washed several times with dry acetonitrile to remove excess Sc(OTf)$_3$. After the final washing, the resulting ME Sc(OTf)$_3$ was dried at 50 °C under vacuum.

Some refinements of the literature procedure are as follows: cooling of the PS/cyclohexane/Sc(OTf)$_3$ solution to room temperature was done at a slow rate (over ca. 1.5 h) by allowing the solution to remain in the oil bath used for heating with the hot plate turned off. When the solution reached room temperature, it was then placed in a water bath to which ice was slowly added over the span of 0.5 h until 0 °C was reached. The addition of hexanes to the solution was performed in a dropwise manner over the course of ca. 20 min.

Solid-State NMR Spectroscopy. Solid-state NMR spectra were obtained on a Varian Infinity Plus NMR spectrometer with an Oxford 9.4 T (ν_0(^{1}H) = 399.73 MHz) wide-bore magnet with ν_0(^{45}Sc) = 97.10 MHz, ν_0(^{13}C) = 100.52 MHz, and ν_0(^{19}F) = 376.09 MHz (University of Windsor). All samples were ground into powders, packed into 4 mm outer diameter (o.d.) zirconium oxide rotors under an inert atmosphere, and sealed with airtight caps. Chemagnetics 4 mm triple-resonance (HXY) or double-resonance (HX) MAS probes were used for all experiments. A detailed list of ^{45}Sc SSNMR acquisition parameters can be found in Supporting Information Tables S1−S6. Scandium chemical shifts were referenced to an aqueous solution of dilute (less than 0.05 M) ScCl$_3$ (δ_{iso} = 0.0 ppm).[37] An echo pulse sequence [π/2−τ_1−θ_{ref}−τ_2−acquire, with θ_{ref} = π/2 or π] was utilized to acquire all ^{45}Sc NMR spectra, and the radiofrequency field of

the pulses, $\nu_1(^{45}\text{Sc})$, was set to ca. one-half of the static central-transition powder pattern width.[56] Static ^{45}Sc NMR spectra of the pure crystalline compounds were acquired with a 90°–90° echo sequence to obtain improved lineshapes and accurately determine tensor parameters (Figure 1). A double-frequency
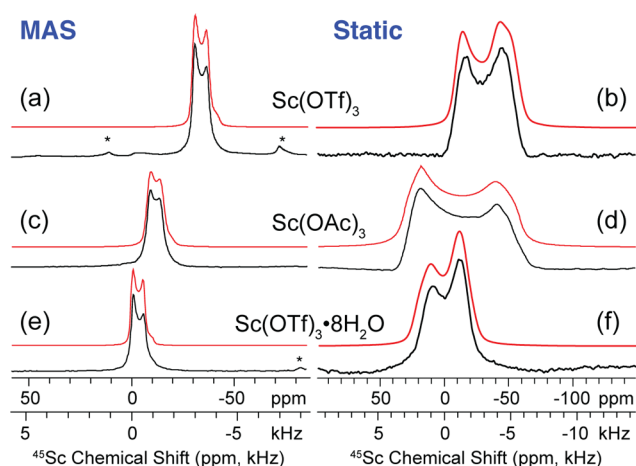

Figure 1. MAS (left) and static (right) ^{45}Sc SSNMR spectra acquired at 9.4 T. Analytical simulations of the spectra (red traces) are overlaid on top of the experimental spectra (black traces). (a) MAS spectrum of Sc(OTf)$_3$ at a sample-spinning rate of ν_{rot} = 4.0 kHz and (b) static spectrum of Sc(OTf)$_3$. (c) MAS spectrum of Sc(OAc)$_3$ at ν_{rot} = 8.0 kHz and (d) static spectrum with ^{1}H decoupling. (e) MAS spectrum of Sc(OTf)$_3$·8H$_2$O at ν_{rot} = 8.0 kHz and (f) static spectrum with ^{1}H decoupling. Spinning sidebands are indicated with asterisks. ^{45}Sc EFG and CS tensor parameters extracted from simulations are listed in Table 1. Static spectra were also acquired at 11.7 T to confirm the ^{45}Sc CS tensor parameters and Euler angles (Supporting Information Figures S1 and S2).

sweep (DFS) sequence[57,58] was applied to enhance the signal of some ^{45}Sc echo spectra of the ME samples. ^{1}H decoupling was applied with $\nu_1(^1\text{H})$ between 22 and 30 kHz, where indicated. Magic-angle spinning (MAS) spectra were acquired with a 90°–90° echo sequence $[\pi/2 - \tau_1 - \pi/2 - \tau_2 - \text{acquire}]$ using high power pulses and large spectral widths. MAS spinning frequencies (ν_{rot}) ranged from 4 to 12 kHz, with interpulse delays equal to $1/\nu_{rot}$. Nonselective pulse widths were adjusted by a factor of $(I + 1/2)^{-1}$ (where I = 7/2) to achieve central-transition (CT) selective ^{45}Sc pulses for all experiments. In general, a large number of scans were acquired for spectra of the ME samples when compared to spectra of the crystalline complexes. The MAS and static ^{45}Sc solid-state NMR spectra were simulated with the WSolids computer program,[59] which uses the Rose convention for Euler angles.[60]

Hydrogen chemical shifts were referenced to neat tetramethylsilane (δ_{iso} = 0.00 ppm) via a secondary standard of adamantane (δ_{iso} = 1.82 ppm). $\pi/2$ pulse widths between 2.3

and 2.4 μs were used corresponding to $\nu_1(^1\text{H})$ = 105–109 kHz. A recycle delay of 20 s was applied for all MAS ^{1}H SSNMR experiments. 32–128 scans were acquired for MAS ^{1}H SSNMR spectra, and MAS frequencies (ν_{rot}) between 10 kHz and 13.5 kHz were used. ^{1}H TRAPDOR MAS SSNMR experiments were acquired with ν_{rot} = 12.5 kHz, and the first echo dephasing period (τ_1) was set to 240 μs. $\nu_1(^{45}\text{Sc})$ of ca. 108 kHz was applied during the echo dephasing period. The control and dephasing spectra were acquired in an interleaved manner, to eliminate any variability in spectrometer performance, which could give rise to false differences in ^{1}H signal intensity. Deconvolutions of MAS ^{1}H SSNMR spectra were performed with a line-fitting routine included in NMR processing software (NUTS, Acorn NMR, Inc.).

Carbon chemical shifts were referenced to neat tetramethylsilane (δ_{iso} = 0.00 ppm) by setting the high-field shift of adamantane (δ_{iso} = 38.57 ppm) as a secondary reference. ^{1}H → ^{13}C variable amplitude[61] cross-polarization MAS (VACP/MAS) SSNMR experiments utilized a contact time between 1 and 5 ms, a pulse delay of 12 s, and ν_{rot} ranged from 6.5 to 13.5 kHz. TPPM decoupling was employed with $\nu_1(^1\text{H})$ of 60–80 kHz.[62] Fluorine chemical shifts were referenced to fluorotrichloromethane (δ_{iso} = 0.00 ppm) by setting the shift of Teflon (δ_{iso} = −122.00 ppm) as a secondary reference. ^{19}F → ^{13}C VACP/MAS NMR experiments utilized a contact time of 2 ms, a pulse delay of 5 s, and a spectral width of 100 kHz.

Additional ^{1}H and ^{19}F experiments on air exposed ME Sc(OTf)$_3$ samples were conducted on an 11.7 T wide-bore Varian NMR spectrometer, which was equipped with a Varian T3 2.5 mm HFXY probe (University of Lethbridge), with 30 dBm isolation between the H and F channels, with additional low-loss (1 dBm) high-power H and F filters in line. ^{1}H–^{19}F and ^{19}F–^{1}H CP/MAS experiments were conducted with contact times between 25 and 8000 μs to probe CP dynamics. Spin locking fields of ca. 60 kHz were applied during CP, and the amplitude of the contact pulse was ramped.[61] TPPM decoupling was applied for either ^{1}H or ^{19}F.[62]

Powder X-ray Diffraction. PXRD patterns were acquired using a Bruker AXS HI-STAR system utilizing a General Area Detector Diffractions System (GADDS). A Cu Kα radiation source (1.540598 Å) with area detector 2θ range of ca. 3°–70° was utilized. Powdered samples were packed in 1.0 mm glass capillaries under an inert atmosphere and flame-sealed to prevent atmospheric exposure. To expose some of the samples to air, the capillary was broken with a pair of tweezers at the flame-sealed (top) side. PXRD patterns were simulated using the Powdercell computer program.[63]

■ RESULTS AND DISCUSSION

Solid-State ^{45}Sc NMR Spectra of Sc(OTf)$_3$, Sc(OAc)$_3$, and Sc(OTf)$_3$·8H$_2$O. Prior to examining the complex ME systems, it is crucial to gain an understanding of the solid-state

Table 1. Experimental ^{45}Sc EFG and CS Tensor Parameters of Crystalline Complexes

compound	C_Q (MHz)[a]	η_q[b]	δ_{iso} (ppm)[c]	Ω (ppm)[d]	κ[e]	α (deg)[f]	β (deg)	γ (deg)
Sc(OAc)$_3$	4.6(2)	0.18(6)	−6.2(8)	73(5)	0.65(10)	0(45)	7(3)	90(45)
Sc(OTf)$_3$	4.7(2)	0.15(10)	−28(1)	26(5)	0.5(2)	35(20)	20(4)	−5(30)
Sc(OTf)$_3$·8H$_2$O	4.2(2)	0.10(10)	1.8(8)	22(5)	0.1(3)	60(90)	22(20)	−75(30)
ME Sc(OTf)$_3$	4.2(2)	0.10(10)	1.8(8)	22(5)	0.1(3)	60(90)	22(20)	−75(30)

[a]$C_Q = eQV_{33}/h$. [b]$\eta_Q = (V_{11} - V_{22})/V_{33}$. [c]$\delta_{iso} = (\delta_{11} + \delta_{22} + \delta_{33})/3$. [d]$\Omega = \delta_{33} - \delta_{11}$. [e]$\kappa = 3(\delta_{22} - \delta_{iso})/\Omega$. [f]The Rose convention is used to describe the Euler angles, which describe the relative orientation of EFG and CS tensors [see refs 59 and 60].
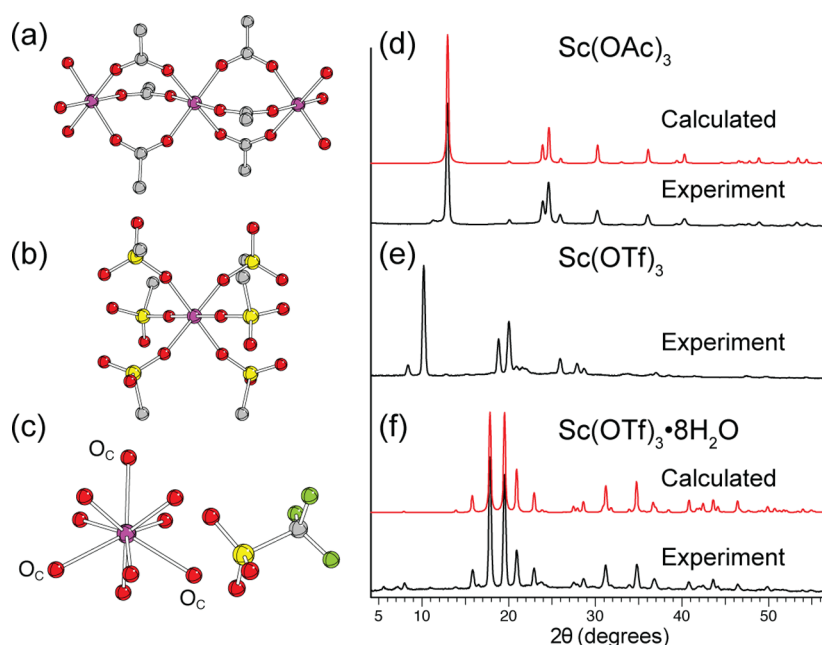
Figure 2. Structures of (a) Sc(OAc)$_3$,[55] (b) hypothesized structural model of Sc(OTf)$_3$, and (c) Sc(OTf)$_3$·8H$_2$O (gray carbon, red oxygen, yellow sulfur, pink scandium, green fluorine).[64] Hydrogen and some fluorine atoms have been omitted for clarity. Experimental (black traces) PXRD patterns of (d) Sc(OAc)$_3$, (e) Sc(OTf)$_3$, and (f) Sc(OTf)$_3$·8H$_2$O. PXRD patterns calculated (red traces) from the corresponding single-crystal X-ray diffraction structures[55,64] are shown for Sc(OAc)$_3$ and Sc(OTf)$_3$·8H$_2$O. The oxygen atoms labeled O$_C$ possess fractional occupancies of 0.67 in the SCXRD structure of Sc(OTf)$_3$·8H$_2$O, leading to eight-coordinate Sc. There is no crystal structure of Sc(OTf)$_3$ available. The model of Sc(OTf)$_3$ presented herein is based upon our ^{45}Sc SSNMR spectra and PXRD patterns.

structures of the anhydrous and hydrated scandium triflate complexes. Anhydrous crystalline scandium(III) trifluoromethanesulfonate [herein referred to as Sc(OTf)$_3$] does not have a known crystal structure due to difficulties in obtaining diffraction-quality single crystals. For this reason, our research group previously performed ^{45}Sc SSNMR and PXRD experiments on Sc(OTf)$_3$, to characterize the scandium coordination environment.[37] The major findings of this previous study are reviewed along with some new data, to clarify some of the structural features of microcrystalline Sc(OAc)$_3$, Sc(OTf)$_3$, and Sc(OTf)$_3$·8H$_2$O prior to discussion of the microencapsulated (ME) systems.

Magic-angle spinning (MAS) and static (i.e., stationary sample) ^{45}Sc SSNMR spectra reveal that the ^{45}Sc quadrupolar parameters of Sc(OTf)$_3$ are similar to those of Sc(OAc)$_3$ (Figure 1, Table 1). We have acquired new static NMR spectra of Sc(OTf)$_3$ at 9.4 and 11.7 T with a 90°−90° echo sequence (Supporting Information Figure S1). This was done because our previous spectra were acquired with a 90°−180° echo sequence and DFS for signal enhancement,[57,58] which can produce nonideal intensities in the static ^{45}Sc SSNMR spectra. As a result, the CS tensor parameters and Euler angles reported herein are slightly different (but within error) from those previously reported by our research group.[37]

Both Sc(OTf)$_3$ and Sc(OAc)$_3$ possess comparable ^{45}Sc EFG tensor parameters (C_Q and η_Q) and CS tensor skew (κ) values, which strongly suggests that the Sc coordination environments are similar for both complexes. A single-crystal X-ray diffraction structure of Sc(OAc)$_3$ has been previously reported,[55] which describes a coordination polymer with bridging acetate groups linking adjacent scandium atoms that reside in pseudooctahedral coordination environments (Figure 2a). The PXRD patterns of Sc(OTf)$_3$ and Sc(OAc)$_3$ (Figure 2d,e) have peaks of similar intensities [although peaks are shifted to

slightly lower 2θ values for Sc(OTf)$_3$], suggesting that the two structures are similar. Because 2θ is inversely proportional to the d-spacings, these differences in 2θ values suggest that the Sc(OTf)$_3$ crystal structure has increased spacings between the diffraction planes of the unit cell as compared to Sc(OAc)$_3$, consistent with the triflate ligands being larger in size than the acetate ligands. The combination of the NMR and PXRD data supports the hypothesis that Sc(OTf)$_3$ is isostructural with Sc(OAc)$_3$ in the solid state, and that Sc(OTf)$_3$ has pseudooctahedral Sc coordination environments, which are formed by six oxygen atoms from six separate triflate ligands. The triflate ligands bridge to neighboring Sc sites to form polymeric chains (i.e., a classic coordination polymer structure, Figure 2b).

Characterization of the hydrated forms of Sc(III) complexes is important, as many anhydrous scandium complexes are hygroscopic and readily form hydrates. For example, several of the commercially purchased samples of anhydrous Sc(OTf)$_3$ were delivered as the hydrated form [Sc(OTf)$_3$·8H$_2$O]. The solid-state structure of Sc(OTf)$_3$·8H$_2$O has been extensively investigated by Sandstrom et al.,[64] who found that the crystal structure of Sc(OTf)$_3$·8H$_2$O has nine water molecules that are coordinated to the Sc atom; however, the oxygen atoms of the water molecules that cap the rectangular faces of the trigonal prism possess fractional occupancies of 0.67 (labeled O$_C$ in Figure 2c),[64] leading to eight-coordinate Sc sites. For these reasons, we have acquired ^{45}Sc SSNMR spectra of the crystalline complex Sc(OTf)$_3$·8H$_2$O (Figure 1e and f). The CS and EFG tensor parameters of Sc(OTf)$_3$·8H$_2$O were confirmed by acquiring static 90°−90° echo ^{45}Sc SSNMR spectra at 9.4 and 11.7 T (Supporting Information Figure S1). The ^{45}Sc SSNMR spectra of Sc(OTf)$_3$·8H$_2$O reveal that the ^{45}Sc EFG and CS tensor parameters are similar to those of Sc(OTf)$_3$ and Sc(OAc)$_3$, with the exception of δ_{iso}, which is +30 ppm more positive than that observed for crystalline

Sc(OTf)$_3$. Most importantly, the ^{45}Sc SSNMR spectra of Sc(OTf)$_3$·8H$_2$O are almost identical in appearance to those of ME Sc(OTf)$_3$ (vide infra).

During the course of this study, we have also identified a new hydrated phase of Sc(OTf)$_3$, which we refer to as Sc(OTf)$_3$·xH$_2$O. Sc(OTf)$_3$·xH$_2$O possesses a PXRD pattern, which is distinct from that of Sc(OTf)$_3$·8H$_2$O (Supporting Information Figure S2a). Further PXRD experiments were performed to identify the order in which the hydrated phases of Sc(OTf)$_3$ are formed. A sample of anhydrous Sc(OTf)$_3$ was packed into a sealed glass capillary, and a PXRD pattern was acquired. The top of the capillary was then broken so that the sample would be exposed to atmospheric moisture. A series of PXRD patterns were then periodically acquired over 30 h (Supporting Information Figure S2a). After ca. 19 h, the PXRD patterns show complete conversion of Sc(OTf)$_3$ to the Sc(OTf)$_3$·xH$_2$O phase, and after ca. 29 h, the PXRD pattern is identical to that of the Sc(OTf)$_3$·8H$_2$O phase. From these PXRD experiments, it is clear that the anhydrous Sc(OTf)$_3$ readily absorbs water and is first converted into the Sc(OTf)$_3$·xH$_2$O phase, followed by adsorption of additional water to form the previously identified Sc(OTf)$_3$·8H$_2$O phase. The Sc(OTf)$_3$·xH$_2$O and Sc(OTf)$_3$·8H$_2$O phases possess identical MAS and static ^{45}Sc SSNMR spectra (Supporting Information Figure S2b), suggesting that both phases possess very similar eight-coordinate scandium environments. MAS ^{1}H and ^{19}F SSNMR spectra of the two hydrated phases are distinct (Supporting Information Figure S2). The MAS ^{1}H SSNMR spectra of Sc(OTf)$_3$·xH$_2$O are much broader than those of Sc(OTf)$_3$·8H$_2$O, suggesting that the ^{1}H nuclei of the water molecules are less mobile in the former. Further investigation of the Sc(OTf)$_3$·xH$_2$O phase is beyond the scope and aim of the current study; however, given the interest in characterizing the hydration state of Sc(III) ions in aqueous solution and the solid state,[64−69] and the role hydrated Sc(III) ions play in aqueous phase catalysis, it merits future study.

^{45}Sc SSNMR Spectra of Microencapsulated (ME) Sc(OTf)$_3$.

We previously acquired ^{45}Sc SSNMR spectra of ME Sc(OTf)$_3$, which revealed a distinct ^{45}Sc isotropic chemical shift of δ_{iso} = 1.8 ppm and a moderate decrease in C_Q in comparison to that of Sc(OTf)$_3$.[37] Our new data reveal that the MAS and static ^{45}Sc SSNMR spectra of ME Sc(OTf)$_3$ are identical to those of Sc(OTf)$_3$·8H$_2$O (Figure 3), as mentioned above. There is usually a large reduction in the signal-to-noise ratios of ^{45}Sc SSNMR spectra of ME Sc(OTf)$_3$ in comparison to those of Sc(OTf)$_3$·8H$_2$O, consistent with the reduced Sc content of the former (ca. 1% Sc by weight, vide infra). If ^{1}H decoupling is not applied during the acquisition of the static ^{45}Sc SSNMR spectra, significant broadening of the static ^{45}Sc central transition powder patterns is observed for both Sc(OTf)$_3$·8H$_2$O and ME Sc(OTf)$_3$ (Figure 3c,f). In the case of crystalline Sc(OTf)$_3$·8H$_2$O, this indicates the presence of relatively large ^{1}H−^{45}Sc dipolar couplings, which arise from the close spatial proximity of the ^{45}Sc nucleus and the ^{1}H nuclei of the coordinated water molecules (Sc−H distances of ca. 2.5−3.0 Å). All of these data suggest that Sc(OTf)$_3$ is hydrated during the microencapsulation process and exists as domains of Sc(OTf)$_3$·8H$_2$O within the polymer, and not as Sc(OTf)$_3$ as previously suggested (although it is possible that the broadening induced by heteronuclear dipolar coupling also arises from proximate ^{1}H nuclei in the surrounding PS, for more discussion vide infra).
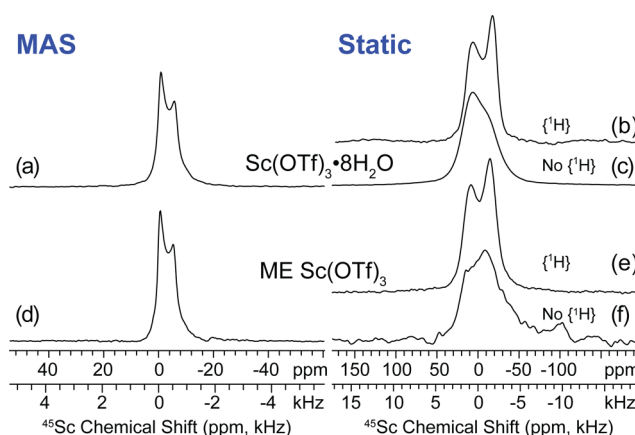

Figure 3. MAS and static ^{45}Sc SSNMR spectra of Sc(OTf)$_3$·8H$_2$O and the commercial sample of ME Sc(OTf)$_3$ acquired at 9.4 T. (a) MAS spectrum of Sc(OTf)$_3$·8H$_2$O at ν_{rot} = 8.0 kHz and (b) static spectra with and (c) without ^{1}H decoupling. (d) MAS spectrum of ME Sc(OTf)$_3$ at ν_{rot} = 12.0 kHz and (e) static spectra with and (f) without ^{1}H decoupling. All static spectra were acquired with a DFS 90°−180° echo pulse sequence.

One initially puzzling aspect of these data was the origin of the hydrating water molecules in the ME Sc(OTf)$_3$ samples. The commercial sample of ME Sc(OTf)$_3$ arrived packed under an argon atmosphere, suggesting that it was prepared under inert conditions; however, we are not absolutely certain of this (the manufacturer would not comment) and cannot provide a definitive explanation for the origin of the water of hydration for this sample. Kobayashi and co-workers' original synthetic procedures for ME Sc(OTf)$_3$ do not call for inert atmosphere synthetic techniques, suggesting that water may be absorbed during preparation of the ME systems.[23] For all of these reasons, we have undertaken the synthesis of our own samples of ME Sc(OTf)$_3$, and characterized them with further SSNMR and PXRD experiments, to confirm the nature of the hydrated Sc^{3+} environments and to posit a source for the hydration water molecules.

MAS and static ^{45}Sc SSNMR spectra for samples of ME Sc(OTf)$_3$ prepared under a variety of conditions are shown in Figure 4 (all syntheses employed dried solvents). The variations in the synthetic procedure include microencapsulating Sc(OTf)$_3$·8H$_2$O under an inert atmosphere (ME-1), and microencapsulation of anhydrous Sc(OTf)$_3$ under an ambient atmosphere (ME-2) or an inert atmosphere (ME-3). It is clear that, regardless of the conditions employed for the synthesis of the ME samples, ^{45}Sc SSNMR spectra similar in appearance to those of Sc(OTf)$_3$·8H$_2$O and the commercial sample of ME Sc(OTf)$_3$ are obtained, excepting the spectra of ME-3 (vide infra).

While the lineshapes of the static and MAS spectra of the ME complexes are similar, the S/N ratios per square root of number of scans of the spectra are variable. For this reason, we have determined the Sc loading levels of the synthesized samples. The integrated intensity (II) and number of scans (NS) for the MAS ^{45}Sc SSNMR spectra of individual samples acquired under identical conditions are listed in Table 2. From these parameters, and knowledge of the total sample mass within the rotor, it is possible to estimate the Sc loading level (Sc wt %) by comparison to the II of MAS ^{45}Sc SSNMR spectra of crystalline Sc(OTf)$_3$·8H$_2$O. The Sc wt % of the ME Sc(OTf)$_3$ samples obtained under different synthetic conditions ranges
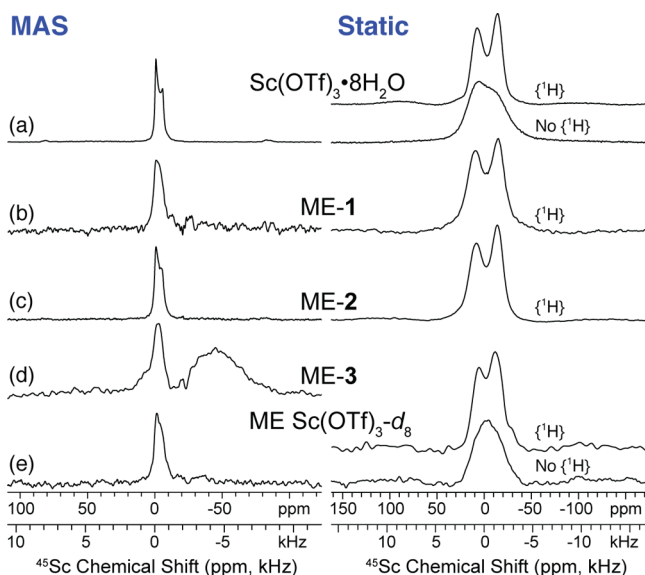
22653

dx.doi.org/10.1021/jp507470v | J. Phys. Chem. C 2014, 118, 22649−22662

Figure 4. MAS (left spectra) and static (right spectra) 9.4 T ^{45}Sc SSNMR spectra of Sc(OTf)$_3$·8H$_2$O and samples of ME Sc(OTf)$_3$ prepared with various synthetic procedures (see text). Spectra of (a) Sc(OTf)$_3$·8H$_2$O, (b) ME Sc(OTf)$_3$ prepared by microencapsulating Sc(OTf)$_3$·8H$_2$O in PS under an inert atmosphere (ME-**1**), (c) ME Sc(OTf)$_3$ prepared by microencapsulating anhydrous Sc(OTf)$_3$ under ambient atmosphere (ME-**2**), (d) ME Sc(OTf)$_3$ prepared by microencapsulating anhydrous Sc(OTf)$_3$ under inert conditions (ME-**3**), and (e) ME Sc(OTf)$_3$ prepared by microencapsulating anhydrous Sc(OTf)$_3$ with fully deuterated PS (ME ScOTf$_3$-d_8) under ambient conditions. All static spectra were acquired with a DFS 90°−90° echo sequence and ^{1}H decoupling (except where noted), and all MAS spectra were acquired with a DFS 90°−180° echo sequence. Static ^{45}Sc SSNMR spectra of Sc(OTf)$_3$·8H$_2$O and ME Sc(OTf)$_3$-d_8 acquired without ^{1}H decoupling are also shown.

from 0.22% (ME Sc(OTf)$_3$-d_8) to 0.90% (ambient ME Sc(OTf)$_3$, ME-**2**). Unfortunately, we do not have any of the commercial sample of ME Sc(OTf)$_3$ remaining from our previous study to determine the Sc wt % by ^{45}Sc SSNMR; however, the manufacturer claims that the sample is ca. 13 wt % Sc(OTf)$_3$ by mass. This corresponds to a Sc wt % of ca. 1.2%, which is similar to the loading levels determined herein for ME-**2**.

The ^{45}Sc SSNMR spectra indicate the presence of domains of Sc(OTf)$_3$·8H$_2$O within the polymer; therefore, it is expected that the Sc loading levels will be low if water of hydration is not supplied during the synthesis. This is clearly the case for ME-**3**, the sample of ME Sc(OTf)$_3$ prepared under inert conditions with anhydrous Sc(OTf)$_3$ (Figure 4d), which has a loading level much lower than that of the other samples (ca. 0.27 Sc wt %). In addition, there is a second broad powder pattern visible in the MAS ^{45}Sc SSNMR spectrum of ME-**3**, which corresponds closely to the spectral region of anhydrous Sc(OTf)$_3$. This is consistent with an absence of water that is required to form significant amounts of the hydrate phase. The small amount of Sc(OTf)$_3$·8H$_2$O visible in ^{45}Sc SSNMR spectrum of ME-**3** likely results from residual water in the solvents, a minor amount of hydrated Sc(OTf)$_3$ mixed in with the anhydrous Sc(OTf)$_3$ and/or from water that entered the reaction flask during the synthetic procedure.

Kobayashi hypothesized that there are bonding interactions between the phenyl groups of PS and the vacant d-orbitals of Sc in ME Sc(OTf)$_3$.[22,30] In our previous ^{45}Sc SSNMR study of ME Sc(OTf)$_3$, we incorrectly attributed the origin of the ^{1}H−^{45}Sc dipolar couplings to spatially proximate ^{1}H nuclei of PS (because we were unaware of the presence of the hydration water molecules), and proposed that there were domains of anhydrous Sc(OTf)$_3$ encapsulated in the polymer.[37] To further confirm the presence of Sc(OTf)$_3$·8H$_2$O, and that the ^{1}H−^{45}Sc dipolar couplings arise from H$_2$O coordinated to the Sc^{3+} ions, we have prepared a sample of ME Sc(OTf)$_3$ with a fully deuterated sample of PS (ca. 98% ^{2}H, we refer to this sample as "ME Sc(OTf)$_3$-d_8"). The static ^{45}Sc SSNMR spectrum of ME Sc(OTf)$_3$-d_8 acquired without ^{1}H decoupling is significantly broadened, indicating that there is still substantial ^{1}H−^{45}Sc dipolar coupling. This confirms that the ^{1}H−^{45}Sc dipolar coupling does not arise solely from proximate ^{1}H nuclei of PS, but rather primarily from coupling to the ^{1}H nuclei of coordinated water molecules. These new data and structural interpretation raise questions about the nature of the interaction between Sc^{3+} and PS in ME samples. It is unlikely that there will be any interactions between the π-systems of the phenyl groups of PS and Sc d-orbitals, as the eight-coordinate hydrated Sc ions are coordinatively saturated. To probe for any interactions with PS, we have acquired MAS ^{1}H and ^{1}H−^{45}Sc TRAPDOR SSNMR spectra (vide infra).

Table 2. Estimates of Sc Loading Levels of ME Sc(OTf)$_3$ Samples

sample	number of scans [NS]	integrated intensity [II][a]	II/NS	m_{tot} (mg)[b]	m_{Sc} (mg)[c]	Sc wt %[d]
Sc(OTf)$_3$·8H$_2$O	64	271	4.234	83	5.9[e]	7.07[e]
ME-**1**	3264	516	0.161	46	0.22	0.49
ME-**2**	752	265	0.352	54	0.49	0.90
ME-**3**	3200	719	0.229[f]	42	0.32	0.27, 0.48[f]
ME Sc(OTf)$_3$-d_8	1376	99	0.072	46	0.10	0.22

[a]The integral was taken over the central transition of a MAS DFS 90°−180° echo spectrum recorded at ν_{rot} = 8.0 kHz for all samples. Identical pulse sequence parameters (e.g., recycle delays, pulse widths, receiver gain) were employed for all samples. All MAS experiments were acquired over the course of 2 days. [b]m_{tot} corresponds to the measured total mass of sample in the rotor. Uncertainties are ±2 mg. [c]m_{Sc} corresponds to the mass of scandium in the rotor. This was found by the following formula: m_{Sc} = 5.87 mg × [(II/NS)$_{Sample}$]/[(II/NS)$_{Sc(OTf)3·8H2O}$]. [d]Sc wt % = 100 × [m_{Sc}]/[m_{tot}]. We estimate uncertainties levels of ca. ±20% of the measured values for the experimentally determined Sc wt %. [e]m_{Sc} and the Sc wt % of the sample of crystalline Sc(OTf)$_3$·8H$_2$O were calculated from the molecular formula and the measured mass of Sc(OTf)$_3$·8H$_2$O in the rotor. [f]This includes integration of the impurity resonance. The first Sc wt % listed corresponds to the resonance attributed to Sc(OTf)$_3$·8H$_2$O, while the second Sc wt % listed corresponds to the resonance attributed to anhydrous Sc(OTf)$_3$. These were determined from the relative integrated intensities of the two resonances in the MAS spectrum. Note that this measure is nonquantitative because the DFS signal enhancement will vary for the two different sites.

MAS ^{1}H SSNMR Spectra of ME Sc(OTf)$_3$. To aid in properly assigning the resonances observed in the MAS ^{1}H SSNMR spectra of ME Sc(OTf)$_3$, MAS ^{1}H SSNMR spectra were also acquired for pristine PS, and PS samples that were treated with the organic solvents that are utilized in the synthesis of ME Sc(OTf)$_3$. The solvent-treated PS samples were obtained by following the procedure for the synthesis of ME Sc(OTf)$_3$, without the addition of any Sc(OTf)$_3$ to the polymer−solvent mixtures. All samples were dried under vacuum at 50 °C.

The MAS ^{1}H SSNMR spectrum of PS acquired at ν_{rot} = 13.5 kHz possesses two broad overlapping resonances (Figure 5a)
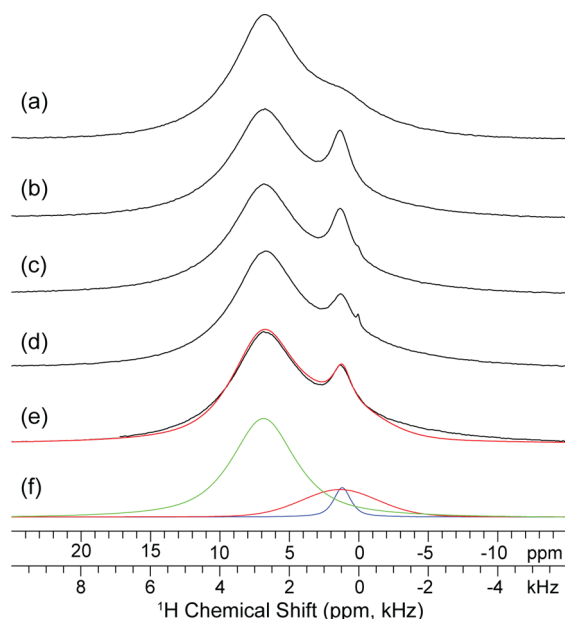

Figure 5. MAS ^{1}H SSNMR spectra of (a) pristine polystyrene (PS), (b) PS recovered from cyclohexane, (c) PS recovered from cyclohexane and hexanes, (d) PS recovered from cyclohexane, hexanes, and acetonitrile, and (e) ambient ME Sc(OTf)$_3$. A fit of the experimental spectrum is shown as the red trace in (e), and three peaks used in the fit are shown in (f). All spectra were acquired with a 90° pulse-acquire sequence, ν_{rot} = 13.5 kHz, 32 scans, and a recycle delay of 20 s. A 20 s pulse delay was required to obtain full longitudinal recovery of magnetization.

attributable to the phenyl protons $[\delta_{iso}(^1H) = 6.9$ ppm, fwhh = 2.2 kHz] and aliphatic protons $[\delta_{iso}(^1H) = 1.4$ ppm, fwhh = 2.6 kHz]. It is not possible to fully resolve the aliphatic and aromatic proton resonances in this sample at this spinning rate due to the strong ^{1}H−^{1}H homonuclear dipolar couplings and the absence of long-range order. The MAS ^{1}H SSNMR spectrum of PS treated with cyclohexane (Figure 5b) contains an additional, comparatively sharp resonance $[\delta_{iso}(^1H) = 1.2$ ppm, fwhh = 0.6 kHz], which obscures the aliphatic proton resonance of PS. The chemical shift of this resonance correlates well with that of neat cyclohexane,[70] and is attributed to cyclohexane absorbed within the polymer. The MAS ^{1}H SSNMR spectra of all subsequent solvent-treated PS samples and ME Sc(OTf)$_3$ are similar to that of PS treated with cyclohexane only (compare Figure 5b to c−e). There are no additional, high-intensity resonances clearly visible in the methyl region (ca. 0.9 ppm) of the MAS ^{1}H NMR spectra, suggesting that acetonitrile and hexanes are not substantially adsorbed within the polymer. ^{13}C SSNMR spectra of the

polymer samples and ME-**2** confirm this (Supporting Information Figure S3). Note that the MAS ^{1}H spectra sometimes show an additional low intensity sharp peak at $\delta_{iso}(^1H) = 0.1$ ppm, which is attributed to the silicone grease used to seal the joints of the Schlenk flask, and which occasionally contaminates some of the samples.[70]

The MAS ^{1}H SSNMR spectrum of ME-**2** (Figure 5e) is similar in appearance to that of the solvent treated PS samples. We have fit the MAS ^{1}H SSNMR spectra of ME-**2** with a line-fitting routine implemented in the NUTS NMR processing software (Figure 5f). The relative integrated intensities are reported with respect to the aromatic peak, which was set to 100 (Table 3). From this deconvolution, the ratio of PS ^{1}H

Table 3. Chemical Shifts and Integrated Intensities of Resonances Employed for Line-Fitting of MAS ^{1}H SSNMR Spectra of ME-2

	line 1	line 2	line 3
δ_{iso} (ppm)	1.20	1.36	6.86
fwhh (kHz)	0.6	2.6	2.2
integrated intensity	6	23	71

nuclei to cyclohexane ^{1}H nuclei is ca. 94:6, indicating an approximate molar ratio of ca. 96:4 (PS monomer unit: cyclohexane). It is not necessary to account for signal from the ^{1}H nuclei of the Sc(OTf)$_3$·8H$_2$O domains, due to the wide breadths of these resonances and the low Sc loading levels (Supporting Information Figure S4). We note that the deconvolutions do not account for intensity dispersed into the spinning sidebands, which may lead to overestimates of the amount of cyclohexane adsorbed in the polymer. In summary, the MAS ^{1}H NMR spectra indicate that a substantial amount of cyclohexane is adsorbed within the polymer during the microencapsulation process.

^{1}H−^{45}Sc TRAPDOR SSNMR Spectra. To determine if there are any interactions between PS/cyclohexane and the domains of Sc(OTf)$_3$·8H$_2$O within ME Sc(OTf)$_3$, we have performed ^{1}H−^{45}Sc TRAPDOR SSNMR experiments. TRAPDOR is a double-resonance pulse sequence that has been extensively used to deduce the spatial proximity of spin-1/2 and quadrupolar nuclei (e.g., ^{1}H and ^{27}Al).[71−73] In the course of a TRAPDOR experiment, two Hahn-echo spectra of the spin-1/2 nucleus (^{1}H) are acquired.[71] The first is acquired in the usual manner (90°−τ_1−180°−τ_2−acquire) and serves as the control experiment, while the second is acquired with irradiation of the quadrupolar nucleus (^{45}Sc) during the first dephasing period (τ_1). If the quadrupolar and spin-1/2 nuclei are dipolar coupled (spatially proximate), then a reduction in signal is observed in the second echo spectrum. The attenuation of the ^{1}H NMR signal generally increases with larger dipolar couplings, smaller quadrupolar coupling constants, longer echo dephasing periods (τ_1), slower spinning rates, and/or higher-power irradiation of the quadrupolar nucleus.[71,72]

^{1}H−^{45}Sc TRAPDOR MAS SSNMR spectra of ME-**2** are shown in Figure 6. Spectra were acquired with sample spinning rate of 12.5 kHz because this afforded a nice compromise between resolution of the ^{1}H spectrum and the amount of dephasing induced by ^{45}Sc irradiation. In addition, with a ν_1 field of ca. 100 kHz, the experiment is well in the adiabatic regime at this spinning rate (adiabaticity parameter, $\alpha \approx 2.4$) where dephasing efficiencies are high. The intensity of the broad patterns in the aromatic region of the ^{1}H−^{45}Sc
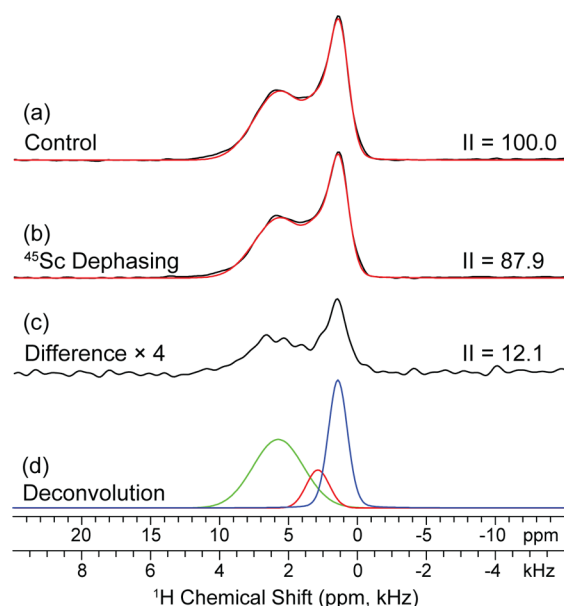
Figure 6. MAS ^{1}H$-^{45}$Sc TRAPDOR SSNMR spectra of ME-**2**, including a (a) control experiment with no ^{45}Sc irradiation, (b) dephasing experiment with irradiation of ^{45}Sc during the τ_1 period, and (c) the difference spectrum resulting from subtraction of the dephasing spectrum from the control spectrum (intensity increased by a factor of 4). Line-fitting simulations (red traces) are overlaid on the experimental spectra (black traces). (d) A deconvolution of the three sites employed in the line-fitting simulations. ν_{rot} = 12.5 kHz and a recycle delay of 20 s were employed.

TRAPDOR spectra of ME-**2** is significantly reduced in comparison to that observed in the Bloch decay spectra of ME-**2** (Figure 5e). This is because ^{1}H nuclei with short effective transverse relaxation time constants (T_2'), such as the PS ^{1}H nuclei, have low intensity in the TRAPDOR spectrum due to the relatively long τ_1 value employed (240 μs).

The integrated intensity (II) of the difference spectrum, obtained by subtracting the ^{1}H$-^{45}$Sc TRAPDOR dephasing spectrum from the control spectrum, is equal to approximately 12% of the II of the control spectrum. This suggests that a substantial fraction of the protons of PS and cyclohexane are dipolar coupled to ^{45}Sc nuclei and are spatially proximate to the Sc(OTf)$_3\cdot$8H$_2$O domains. The amount of dephasing observed in the TRAPDOR spectra and the relatively low loading level of Sc within the sample (0.90 Sc wt %) suggest that Sc(OTf)$_3\cdot$8H$_2$O must be uniformly dispersed throughout the polymer in nanometer scale domains. This is the only way to create a sizable number of dipolar contacts between ^{1}H and ^{45}Sc nuclei, which in turn leads to significant dephasing in ^{1}H$-^{45}$Sc TRAPDOR experiments. These findings are entirely consistent with previous SEM-EDX images of ME Sc(OTf)$_3$, which show that Sc is homogeneously dispersed over the polymer surface in submicrometer size domains.[23]

Deconvolutions of the ^{1}H$-^{45}$Sc TRAPDOR spectra of ambient ME Sc(OTf)$_3$ were performed to see if the individual resonances experience differing degrees of dephasing. The ^{1}H spectra could be effectively fit with three individual resonances, for which the δ_{iso}, fwhh, and II of the individual resonances are listed in Table 4. Because of transverse relaxation, the δ_{iso} and II values obtained from deconvolution of the TRAPDOR spectra are different from those obtained from the Bloch decay spectra. From examination of the II values for the control and

Table 4. Chemical Shifts and Integrated Intensities of Resonances Employed for Line-Fitting of MAS ^{1}H$-^{45}$Sc TRAPDOR NMR Spectra of ME-2

	line 1	line 2	line 3
δ_{iso} (ppm)	1.41	2.87	5.74
fwhh (kHz)	0.65	0.8	1.7
II$_{Control}$	25.3	70.4	100.0
II$_{Dephasing}$	23.1	61.6	87.3
ΔII^a	0.13	0.09	0.13

$^a\Delta$II = (II$_{Control}$ − II$_{Dephasing}$)/II$_{Control}$.

dephasing experiments, it appears that the signal intensity of the ^{1}H resonances, which correspond to cyclohexane and the PS phenyl groups, undergoes the greatest degree of dephasing (signal reduction of ca. 13%), while the resonance that corresponds to the aliphatic PS undergoes a slightly lesser degree of dephasing (signal reduction of ca. 9%). This would suggest that the cyclohexane molecules and the phenyl groups of PS make the closest contacts with the Sc(OTf)$_3\cdot$8H$_2$O domains; however, given the poor resolution and the error inherent to the line fitting routines, these results are not conclusive.

^{1}H$-^{45}$Sc TRAPDOR NMR spectra of ME Sc(OTf)$_3$-d_8 were also acquired, because spectral resolution should be improved by isotopic dilution of the ^{1}H nuclei (Supporting Information Figure S5). These spectra show a total II decrease of ca. 9.7% when ^{45}Sc irradiation is applied, consistent with observations for the nondeuterated sample. However, site-specific measurements of dephasing remain challenging, due to the low S/N of the aromatic portion of the spectrum, and the overlap between the strong (protonated) cyclohexane and weak aliphatic resonances. Hence, TRAPDOR spectra of this sample indicate spatial proximity of the Sc-containing nanodomains and the PS, but cannot be used quantitatively to model the precise structural positions of these domains with respect to one another.

Additional ^{19}F, ^{13}C, and ^{2}H SSNMR Experiments. Several ^{2}H, ^{13}C, and ^{19}F SSNMR experiments were performed on ME Sc(OTf)$_3$; however, these experiments provided little new information on the molecular structure of the complex (Supporting Information Figures S6 and S7), but are consistent with our current structural hypotheses. A brief discussion of these results is presented in the Supporting Information for the interested reader.

Powder X-ray Diffraction. The static and MAS ^{45}Sc SSNMR spectra of ME Sc(OTf)$_3$ possess sharp spectral features, which are indicative of ordered, crystalline domains of Sc(OTf)$_3\cdot$8H$_2$O. PXRD experiments were conducted on ME-**1** and ME-**2** to confirm the presence of crystalline domains within the polymer. The PXRD patterns of the two samples (Figure 7) possess sharp peaks overlaid on a broad underlying peak. The intensities and positions of the peaks observed in the PXRD patterns of ME-**1** and ME-**2** closely match those of the crystalline hydrate phases, Sc(OTf)$_3\cdot$8H$_2$O and Sc(OTf)$_3\cdot$xH$_2$O, respectively. The shape and position of the broad underlying peaks observed in the PXRD pattern of both ME Sc(OTf)$_3$ samples is similar to that observed in the PXRD pattern of solvent-treated PS (Figure 7f). The PXRD patterns of both ME Sc(OTf)$_3$ samples also indicate the absence of any anhydrous Sc(OTf)$_3$. In summary, the PXRD experiments are also consistent with the incorporation of Sc(OTf)$_3$ as nanocrystalline domains of Sc(OTf)$_3\cdot$8H$_2$O/Sc(OTf)$_3\cdot$xH$_2$O
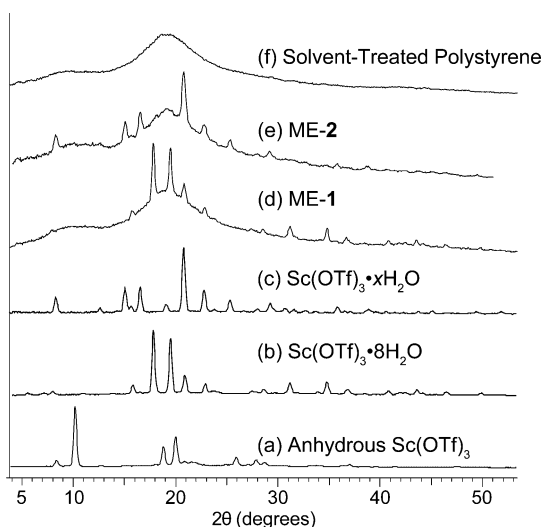
Figure 7. Experimental PXRD patterns obtained from (a) anhydrous $Sc(OTf)_3$, (b) $Sc(OTf)_3 \cdot 8H_2O$, (c) $Sc(OTf)_3 \cdot xH_2O$, (d) ME-**1**, (e) ME-**2**, and (f) solvent-treated PS.

Figure 8. MAS ^1H SSNMR spectra (left) and static (right) ^{45}Sc SSNMR 90°−180° echo spectra of a sample of ambient ME-**2**, which has been exposed to air. The sample was exposed to air for total times of (a) 0 h, (b) 20 h, (c) 2 days, and (d) 15 days. For exposure times of 20 h and 2 days, the static ^{45}Sc SSNMR spectra are shown with and without ^1H decoupling. For the exposure time of 15 days, the static ^{45}Sc SSNMR spectra were acquired with selective and nonselective 90° pulses.

in ME $Sc(OTf)_3$, the degree of which is highly dependent upon the exposure to atmospheric moisture, hydrated solvent, etc. (vide infra).

Exposure of ME $Sc(OTf)_3$ to Ambient Moisture. When ME $Sc(OTf)_3$ is employed as a catalyst, it will likely be exposed to water contained in organic solvents employed as the reaction media, as well as to atmospheric moisture; hydrated ME $Sc(OTf)_3$ may be more representative of the structure of the working catalyst. While all of the samples of ME $Sc(OTf)_3$ were handled under an inert atmosphere, it is worthwhile to examine the influence of moisture adsorption on the catalyst structure. A sample of ME-**2** packed into a rotor was exposed to ambient atmosphere by removing the airtight cap at the top of the pencil-style rotor. The sample was then left on the benchtop for ca. 20 h, and the sample was then capped and SSNMR spectra were acquired.

^1H and ^{45}Sc SSNMR spectra of this air-exposed sample of ME-**2** are shown in Figure 8. After 20 h of air exposure, an additional relatively sharp resonance is visible in the MAS ^1H SSNMR spectrum (δ_{iso} = 6.3 ppm), indicating that ME-**2** has absorbed water from the atmosphere. The observed δ_{iso} value indicates that the water is associated with the $Sc(OTf)_3 \cdot 8H_2O$ domains, and the narrow width of the resonance implies that the water possesses significant rotational/translational freedom. Despite the adsorbed water, the ^{45}Sc SSNMR spectra are similar to those of ME-**2** handled under an inert atmosphere (compare Figure 8a and b). ^1H−^{45}Sc TRAPDOR SSNMR spectra indicate that there is still significant dephasing in the ^{45}Sc irradiation spectrum (Supporting Information Figure S8), suggesting that the $Sc(OTf)_3 \cdot 8H_2O$ domains are still intact and dispersed throughout the polymer.

After 2 days of total air exposure time, the ^1H resonance corresponding to water is further increased in intensity. The static ^{45}Sc SSNMR spectra of ME-**2** begin to show substantial differences from those of the pristine ME-**2**. The static powder patterns are similar, which indicates that the eight-coordinate Sc environments are retained; however, the spectrum of ME-**2** acquired without decoupling displays a sharp central feature, which may be indicative of self-decoupling of the ^1H nuclei. This self-decoupling may occur due to rapid exchange of water
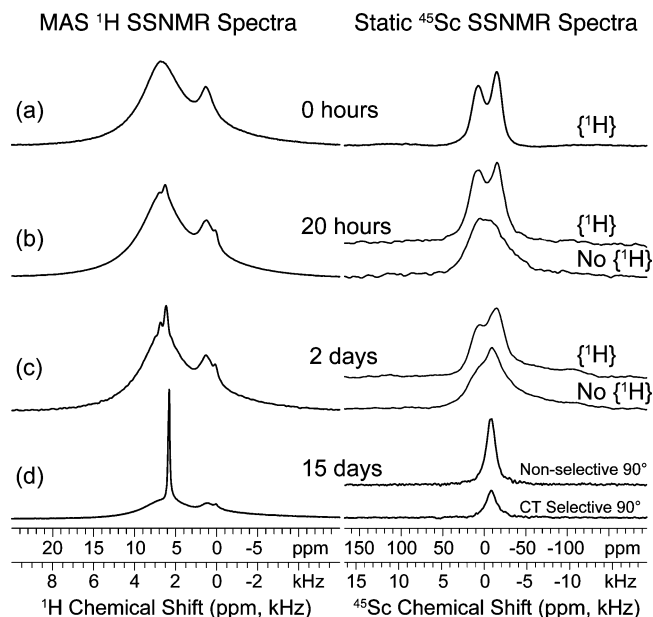
molecules between the first and second scandium coordination spheres.

Finally, after 15 days of total exposure time, the MAS ^1H SSNMR spectra indicate that substantially more water has been absorbed. The water resonance is very narrow and intense, and observed at δ_{iso} = 5.8 ppm, which is closer to that of liquid water (ca. 4.8 ppm). The static ^{45}Sc SSNMR spectra show a single relatively narrow resonance (fwhh of ca. 1 kHz) with δ_{iso} = −6.3 ppm. The static ^{45}Sc SSNMR spectra were acquired with central transition selective and nonselective 90° pulses, and it is clear that the nonselective 90° pulses give maximum signal. This indicates that the Sc^{3+} ions have entered a solution-like phase where the quadrupolar interaction is averaged by molecular motion. Furthermore, ^1H−^{45}Sc TRAPDOR SSNMR spectra show essentially no dephasing when ^{45}Sc irradiation is applied, likely because the mobility of the Sc^{3+} ions and water molecules efficiently averages ^1H−^{45}Sc dipolar couplings (Supporting Information Figure S8).

PXRD experiments were also performed on a sample of air-exposed ME $Sc(OTf)_3$ to monitor the hydration process. A sample of ME-**2** was packed into a flame-sealed glass capillary under an inert atmosphere. The capillary was mounted in the diffractometer, and the top of the capillary was then broken to expose the sample to atmospheric moisture. PXRD patterns were acquired periodically (Figure 9). Initially, there are crystalline domains of $Sc(OTf)_3 \cdot xH_2O$ within ME-**2**. After ca. 24 min of air exposure, conversion to crystalline domains of $Sc(OTf)_3 \cdot 8H_2O$ occurs. As further moisture is absorbed, the intensities of the diffraction peaks decrease until the pattern matches that of solvent-treated PS (at ca. 13.5 h), which indicates that the crystalline domains have been converted into amorphous domains (and/or dissolved by excess water). We note that the timings of the structural differences observed by
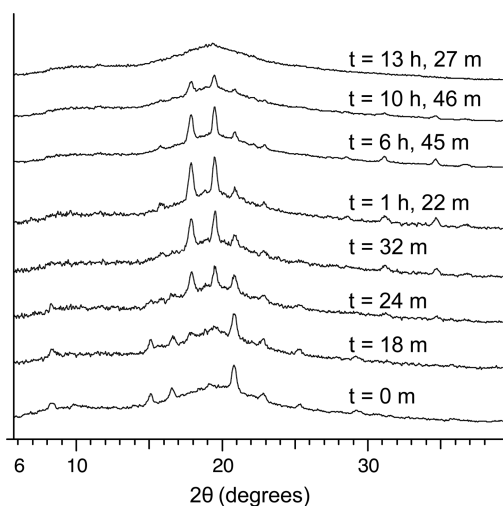
Figure 9. PXRD patterns acquired from a sample of ME Sc(OTf)$_3$ prepared under ambient conditions (ME-**2**), which was exposed to air at the start of the PXRD measurements. The total exposure time is listed to the right of each PXRD pattern.

Figure 10. MAS ^{1}H{^{19}F} and ^{19}F{^{1}H} SSNMR spectra of air exposed ME-**2** acquired with ν_{rot} = 21000 Hz at 11.7 T. Spectra were acquired after 1, 6, and 12 days of sample spinning. The ^{1}H spectra were acquired with direct polarization (a and c) or CP from ^{19}F (b and d), and ^{19}F spectra were acquired with direct polarization (e, g, and h) or CP from ^{1}H (f and i). ^{1}H or ^{19}F TPPM decoupling was applied where appropriate. For the CP spectra, contact times greater than 0.5 ms were employed.

PXRD and SSNMR are different, because the sample was tightly packed into the rotor for SSNMR experiments, while in the PXRD capillary, the flakes of ME-**2** are loosely packed, permitting easy diffusion of air through the sample and resulting in faster absorption of moisture.

^{1}H−^{19}F and ^{19}F−^{1}H Cross-Polarization Experiments on Air-Exposed ME Sc(OTf)$_3$. To further probe the structure and hydration dynamics of hydrated ME Sc(OTf)$_3$, ^{1}H−^{19}F and ^{19}F−^{1}H CP/MAS spectra of air-exposed ME-**2** were acquired. The ^{1}H direct polarization and ^{19}F−^{1}H CP/MAS SSNMR spectra of the air-exposed ME-**2** are shown in Figure 10a and b, respectively. The direct-polarization ^{1}H SSNMR spectrum is similar to that previously observed for air exposed ME-**2** (Figure 8d); a narrow resonance at $\delta_{iso}(^1$H) = 5.9 ppm (attributed to excess adsorbed water) lies on top of the relatively broad resonances of PS.

Despite the fact that the water molecules are relatively mobile (as indicated by the breadth of the ^{1}H resonance and CP dynamics, vide infra), it is possible to utilize CP from ^{19}F to excite the water resonance (Figure 10b). The ^{19}F−^{1}H CP spectrum is distinct from the direct polarization ^{1}H spectrum and only shows the resonances associated with the adsorbed water. This suggests that some of the excess water is likely located near the Sc(OTf)$_3$ domains. The ^{19}F direct polarization and ^{1}H−^{19}F CP SSNMR spectra (Figure 10e and f, respectively) are similar and possess single peaks composed of two overlapping components. One component is centered at $\delta_{iso}(^{19}$F) = −78.9 ppm, and the other is centered at $\delta_{iso}(^{19}$F) = −77.9 ppm. These chemical shifts are similar to those observed for crystalline Sc(OTf)$_3$·8H$_2$O and Sc(OTf)$_3$·xH$_2$O, respectively (Supporting Information Figure S2). Measurement of the ^{1}H−^{19}F CP dynamics indicates that the ^{19}F CP signal from the Sc(OTf)$_3$·xH$_2$O domains (−77.9 ppm) builds up more quickly than the CP signal from the Sc(OTf)$_3$·8H$_2$O domains (Supporting Information Figure S9). The faster CP signal build-up rate, and reduced proton rotating frame relaxation time constant ($T_{1\rho}(^1$H)), are consistent with reduced mobility of water protons in the Sc(OTf)$_3$·xH$_2$O phase as compared to the Sc(OTf)$_3$·8H$_2$O phase. This is also consistent with all
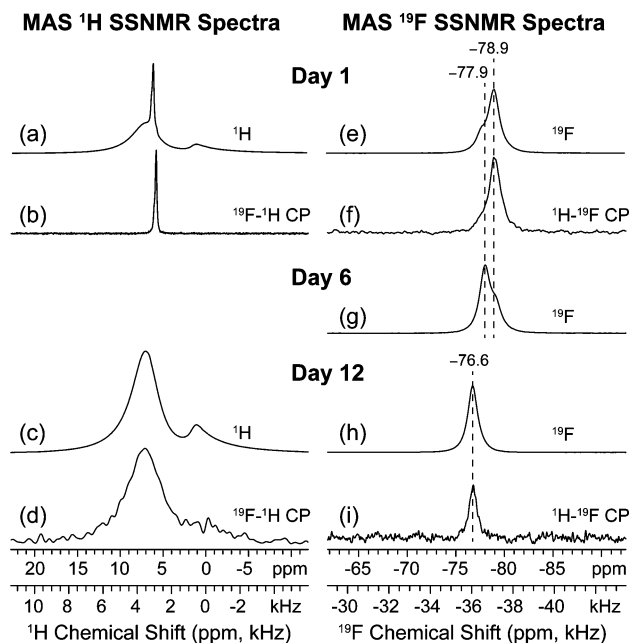
previous observations, which indicate that the Sc(OTf)$_3$·8H$_2$O phase might contain additional excess waters of hydration.

Solid-state NMR experiments at 11.7 T on air-exposed ME-**2** were performed over 2 weeks. After ca. 6 days of sample spinning, the MAS ^{19}F spectra of the air-exposed ME-**2** showed an increase in the intensity of the resonance at $\delta_{iso}(^{19}$F) = −77.9 ppm attributed to Sc(OTf)$_3$·xH$_2$O (Figure 10g). During these experiments, the sample was spun with dry nitrogen gas in an imperfectly sealed 2.5 mm rotor; therefore, it is likely that the excess moisture was removed from the sample by the continuous flow of dry N$_2$ gas. This results in an increase in the intensity of the Sc(OTf)$_3$·xH$_2$O ^{19}F resonances. This sample is now referred to as dehydrated ME-**2**.

After ca. 12 days of sample spinning, dramatically different MAS ^{19}F and ^{1}H SSNMR spectra of dehydrated ME-**2** were observed. The narrow intense ^{1}H peak attributed to adsorbed water is no longer present (compare Figure 10a and b to c and d, respectively), and the spectra are similar to those obtained prior to air exposure (Figure 5). The ^{19}F spectra display a single resonance at $\delta_{iso}(^{19}$F) = −76.6 ppm (Figure 10h), which is the same chemical shift that was observed for crystalline anhydrous Sc(OTf)$_3$. These spectra confirm that the adsorption of water by the Sc(OTf)$_3$ crystals within the polymer is reversible and that dehydrated/anhydrous ME-**2** has formed.

^{1}H−^{19}F and ^{19}F−^{1}H CP experiments are useful for establishing spatial proximities of the polymer to the triflate groups in dehydrated form of ME-**2**. While the direct excitation MAS ^{19}F spectrum indicates that only anhydrous Sc(OTf)$_3$ is present, the ^{1}H−^{19}F CP/MAS spectrum (Figure 10i) demonstrates that there are still ^{1}H nuclei close enough for CP transfer to the ^{19}F nuclei of the triflate groups. Similarly, CP from ^{19}F can be used to obtain a MAS ^{1}H SSNMR spectrum.

This ^{19}F–^{1}H CP/MAS spectrum only contains aromatic resonances of PS (Figure 10d).[74] This suggests that in this dehydrated form of ME-**2** there may be an interaction between the aromatic groups of PS and the Sc(OTf)$_3$ domains, consistent with Kobayashi's original hypotheses concerning the structure of ME Sc(OTf)$_3$.

CONCLUSIONS

^{45}Sc SSNMR spectra of the pure crystalline forms of Sc(OTf)$_3$ and Sc(OTf)$_3$·8H$_2$O have been acquired. A new hydrated phase of Sc(OTf)$_3$, Sc(OTf)$_3$·xH$_2$O, has been identified. ME Sc(OTf)$_3$ has been investigated by multinuclear SSNMR and PXRD experiments, and a structural model of the ME Sc(OTf)$_3$ system is now proposed (Figure 11). ^{45}Sc SSNMR
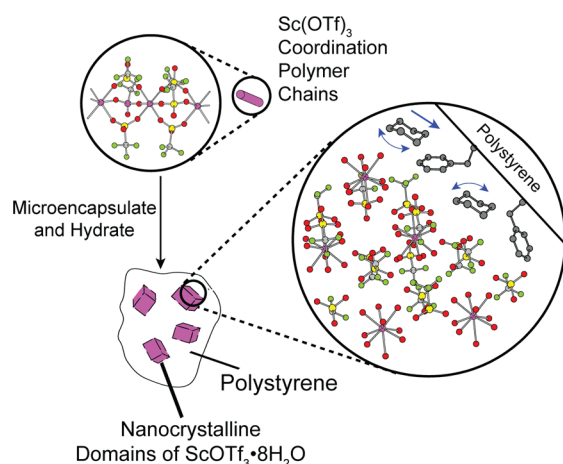

Figure 11. Proposed structural model of ME Sc(OTf)$_3$. Anhydrous Sc(OTf)$_3$ is hydrated when it undergoes microencapsulation in PS, resulting in the formation of nanocrystalline domains of Sc(OTf)$_3$·8H$_2$O in the polymer. The PS groups and cyclohexane molecules are spatially proximate to the surface of the nanocrystalline Sc(OTf)$_3$·8H$_2$O domains. The cyclohexane molecules undergo translational and rotational motions (indicated by the blue arrows).

spectra indicate that Sc(OTf)$_3$ is incorporated into PS as domains of Sc(OTf)$_3$·8H$_2$O and/or Sc(OTf)$_3$·xH$_2$O, the relative amounts of which depend upon the level of hydration during synthesis or upon exposure of ME Sc(OTf)$_3$ to ambient moisture. ^{1}H and ^{13}C SSNMR spectra show that a substantial amount of cyclohexane is also incorporated into ME Sc(OTf)$_3$, but other solvents used in preparation of the ME samples are not present in any significant amounts. ^{1}H–^{45}Sc TRAPDOR experiments indicate that scandium is dispersed throughout the polymer, consistent with SEM-EDX images previously acquired by Kobayashi.[23] However, PXRD experiments reveal that the diffraction patterns of ME Sc(OTf)$_3$ are similar to those of the crystalline complexes, Sc(OTf)$_3$·8H$_2$O and Sc(OTf)$_3$·xH$_2$O, suggesting that scandium must be dispersed throughout the polymer in nanocrystalline domains. Hence, the structure of this system is best described as a composite material, where nanocrystalline domains of inorganic material are dispersed throughout the polymer.[75–80] There is no evidence of a direct interaction between the phenyl groups of PS and the scandium centers in hydrated ME Sc(OTf)$_3$; rather, it is most likely that Sc(OTf)$_3$·8H$_2$O is stabilized in the PS matrix by physisorption (i.e., physical envelopment). It is possible, though not confirmed directly by this work, that hydrogen-bonding interactions between water molecules at the surface of the

Sc(OTf)$_3$·8H$_2$O/Sc(OTf)$_3$·xH$_2$O domains and the phenyl groups are key to stabilizing the structure of ME Sc(OTf)$_3$, because contact angle measurements on oriented PS films and AFM studies of PS surfaces indicate that phenyl group surfaces are slightly hydrophilic in comparison to alkyl groups.[81,82] This could also explain why Sc loading levels are higher when PS is used for microencapsulation instead of polybutadiene or polyethylene. Finally, ^{1}H and ^{19}F CP/MAS experiments demonstrate that hydration of the Sc(OTf)$_3$·8H$_2$O domains within the polymer is reversible and that upon dehydration there is still contact between PS and the Sc(OTf)$_3$ domains.

The newly proposed structural model for ME Sc(OTf)$_3$ is clearly different from previous models, and may provide insight into the structure and chemistry of the numerous heterogeneous scandium catalysts, which have been prepared utilizing a number of different schemes.[21,83–85] Future studies of ME Sc(OTf)$_3$ should focus on correlating the hydration state and Sc(OTf)$_3$ domain sizes to the observed catalytic activities to better obtain defined structure–activity relationships. The multinuclear SSNMR and PXRD experiments described herein are clearly applicable for the characterization of such systems, and should aid in the future design of new scandium-based catalysts, as well a variety of ME catalysts involving different types of metals.[22,85–97]

ASSOCIATED CONTENT

Ⓢ Supporting Information

Additional details of SSNMR experiments, additional ^{1}H, ^{2}H, ^{13}C, ^{19}F, and ^{45}Sc SSNMR spectra, and PXRD patterns. This material is available free of charge via the Internet at http://pubs.acs.org.

AUTHOR INFORMATION

Corresponding Author

*Fax: (519) 973-7098. E-mail: rschurko@uwindsor.ca. Web: http://www.uwindsor.ca/schurko.

Notes

The authors declare no competing financial interest.

ACKNOWLEDGMENTS

■ REFERENCES

(1) Anastas, P. T.; Warner, J. C. *Green Chemistry: Theory and Practice*; Oxford University Press: New York, 1998.

(2) Anastas, P. T.; Heine, L. G.; Williamson, T. C. *Green Chemical Synthesis and Processes*; American Chemical Society: Washington, DC, 2000.

(3) Anastas, P. T.; Kirchhoff, M. M.; Williamson, T. C. Catalysis as a Foundational Pillar of Green Chemistry. *Appl. Catal., A* 2001, 221, 3−13.

(4) Anastas, P. T.; Kirchhoff, M. M. Origins, Current Status, and Future Challenges of Green Chemistry. *Acc. Chem. Res.* 2002, 35, 686−694.

(5) Breslow, R. In *Green Chemistry: Frontiers in Benign Chemical Syntheses and Processes*; Anastas, P. T., Williamson, T. C., Eds.; Oxford University Press: New York, 1998.

(6) Li, C. J. In *Green Chemical Syntheses and Processes*; Anastas, P. T., H. L., G., Williamson, T. C., Eds.; American Chemical Society: Washington, DC, 2000.

(7) Li, C. J. Organic Reactions in Aqueous Media With a Focus on Carbon-Carbon Bond Formations: A Decade Update. *Chem. Rev.* 2005, 105, 3095−3165.

(8) Hachiya, I.; Kobayashi, S. Aqueous Reactions with a Lewis-Acid and an Organometallic Reagent - the Scandium Trifluoromethanesulfonate-Catalyzed Allylation Reaction of Carbonyl-Compounds with Tetraallyltin. *J. Org. Chem.* 1993, 58, 6958−6960.

(9) Kobayashi, S.; Hachiya, I.; Ishitani, H.; Araki, M. Scandium Trifluoromethanesulfonate $(Sc(OTf)_3)$ as a Novel Reusable Lewis-Acid Catalyst in Aldol and Michael Reactions. *Synlett* 1993, 472−474.

(10) Kawada, A.; Mitamura, S.; Kobayashi, S. Scandium Trifluoromethanesulfonate - a Novel Catalyst for Friedel-Crafts Acylation. *Synlett* 1994, 545−546.

(11) Kobayashi, S. Rare-Earth-Metal Trifluoromethanesulfonates as Water-Tolerant Lewis-Acid Catalysts in Organic-Synthesis. *Synlett* 1994, 689−701.

(12) Kobayashi, S.; Araki, M.; Ishitani, H.; Nagayama, S.; Hachiya, I. Activation of Imines by Rare-Earth-Metal Triflates - $Ln(OTf)_3$- or $Sc(OTf)_3$-Catalyzed Reactions of Imines with Silyl Enolates and Diels-Alder Reactions of Imines. *Synlett* 1995, 233−234.

(13) Kobayashi, S.; Araki, M.; Yasuda, M. One-Pot Synthesis of Beta-Amino Esters from Aldehydes Using Lanthanide Triflate as a Catalyst. *Tetrahedron Lett.* 1995, 36, 5773−5776.

(14) Kobayashi, S.; Ishitani, H.; Nagayama, S. Lanthanide Triflate Catalyzed Imino Diels-Alder Reactions - Convenient Syntheses of Pyridine and Quinoline Derivatives. *Synthesis* 1995, 1195.

(15) Kobayashi, S.; Ishitani, H.; Nagayama, S. $Ln(OTf)_3$-Catalyzed or $Sc(OTf)_3$-Catalyzed 3 Components Coupling Reactions between Aldehydes, Amines, and Dienes or Alkenes - Efficient Syntheses of Pyridine and Quinoline Derivatives. *Chem. Lett.* 1995, 423−424.

(16) Kobayashi, S.; Ishitani, H.; Ueno, M. Facile Synthesis of Alpha-amino Nitriles Using Lanthanide Triflate as a Lewis Acid Catalyst. *Synlett* 1997, 115.

(17) Kobayashi, S.; Nagayama, S. Aldehydes vs aldimines. Unprecedented Aldimine-Selective Nucleophilic Additions in the Coexistence of Aldehydes Using a Lanthanide Salt as a Lewis Acid Catalyst. *J. Am. Chem. Soc.* 1997, 119, 10049−10053.

(18) Kobayashi, S. Scandium Triflate in Organic Synthesis. *Eur. J. Org. Chem.* 1999, 15−27.

(19) Kobayashi, S.; Sugiura, M.; Kitagawa, H.; Lam, W. W. L. Rare-earth Metal Triflates in Organic Synthesis. *Chem. Rev.* 2002, 102, 2227−2302.

(20) Fringuelli, F.; Piermatti, O.; Pizzo, F.; Vaccaro, L. Recent Advances in Lewis Acid Catalyzed Diels-Alder Reactions in Aqueous Media. *Eur. J. Org. Chem.* 2001, 439−455.

(21) Luo, S. Z.; Zhu, L. H.; Talukdar, A.; Zhang, G. H.; Mi, X. L.; Cheng, J. P.; Wang, P. G. Recent Advances in Rare Earth-metal Triflate Catalyzed Organic Synthesis in Green Media. *Mini-Rev. Org. Chem.* 2005, 2, 177−202.

(22) Akiyama, R.; Kobayashi, S. "Microencapsulated" and Related Catalysts for Organic Chemistry and Organic Synthesis. *Chem. Rev.* 2009, 109, 594−642.

(23) Kobayashi, S.; Nagayama, S. A Microencapsulated Lewis Acid. A New Type of Polymer-Supported Lewis Acid Catalyst of Wide Utility in Organic Synthesis. *J. Am. Chem. Soc.* 1998, 120, 2985.

(24) Schager, F.; Bonwrath, W. Synthesis of D,L-α-tocopherol Using "Microencapsulated" Catalysts. *Appl. Catal., A* 2002, 202, 117.

(25) Suzuki, T.; Watahiki, T.; Oriyama, T. A Novel and Efficient Method for the Silylation of Alcohols with Methallylsilanes Catalyzed by $Sc(OTf)_3$. *Tetrahedron Lett.* 2000, 41, 8903−8906.

(26) Kobayashi, S.; Komoto, I.; Matsuo, J. Catalytic Friedel-Crafts Acylation of Aniline Derivatives. *Adv. Synth. Catal.* 2001, 343, 71.

(27) Olah, G. A. *Friedel-Crafts Chemistry*; Wiley-Interscience: New York, 1973.

(28) Heaney, H. In *Comprehensive Organic Synthesis*; Trost, B. M., Ed.; Pergamon Press: Oxford, 1991; Vol. 2, p 733.

(29) Olah, G. A.; Krishnamurti, R.; Prakash, G. K. S. In *Comprehensive Organic Synthesis*; Trost, B. M., Ed.; Pergamon Press: Oxford, U.K., 1991; Vol. 3, p 293.

(30) Kobayashi, S.; Akiyama, R. Renaissance of Immobilized Catalysts. New Types of Polymer-supported Catalysts, "Microencapsulated Catalysts", Which Enable Environmentally Benign and Powerful High-throughput Organic Synthesis. *Chem. Commun.* 2003, 449−460.

(31) Spiess, H. W. Structure and Dynamics of Solid Polymers from 2D-NMR and 3D-NMR. *Chem. Rev.* 1991, 91, 1321−1338.

(32) Schmidt-Rohr, K.; Spiess, H. W. *Multidimensional Solid-State NMR and Polymers*; Academic Press: London, 1994.

(33) Brown, S. P.; Spiess, H. W. Advanced Solid-state NMR Methods for the Elucidation of Structure and Dynamics of Molecular, Macromolecular, and Supramolecular Systems. *Chem. Rev.* 2001, 101, 4125−4155.

(34) Tien, C.; Charnaya, E. V.; Sun, S. Y.; Wu, R. R.; Ivanov, S. N.; Khazanov, E. N. Al-27 and Sc-45 NMR Studies of the $Y_3Sc_xAl_5-xO_{12}$ Mixed Garnets. *Phys. Status Solidi B* 2002, 233, 222−229.

(35) Laguta, V. V.; Glinchuk, M. D.; Nokhrin, S. N.; Bykov, I. P.; Blinc, R.; Gregorovic, A.; Zalar, B. NMR Study of Local Structure and Chemical Ordering in $PbMg_{1/3}Nb_{2/3}O_3$ and $PbSc_{1/2}Nb_{1/2}O_3$ Relaxor Ferroelectrics. *Phys. Rev. B* 2003, 67, 104106.

(36) Laguta, V. V.; Glinchuk, M. D.; Bykov, I. P.; Blinc, R.; Zalar, B. NMR Study of Ionic Shifts and Polar Ordering in the Relaxor Ferroelectric $Pb(Sc_{1/2}Nb_{1/2})O_3$. *Phys. Rev. B* 2004, 69, 054103.

(37) Rossini, A. J.; Schurko, R. W. Experimental and Theoretical Studies of Sc-45 NMR Interactions in Solids. *J. Am. Chem. Soc.* 2006, 128, 10391−10402.

(38) Khabibulin, D.; Romanenko, K.; Zuev, M.; Lapina, O. Solid State NMR Characterization of Individual Compounds and Solid Solutions Formed in Sc_2O_3-V_2O_5-Nb_2O_5-Ta_2O_5 System. *Magn. Reson. Chem.* 2007, 45, 962−970.

(39) Kim, N.; Stebbins, J. F.; Quartieri, S.; Oberti, R. Scandium-45 NMR of Pyrope-Grossular Garnets: Resolution of Multiple Scandium Sites and Comparison with X-ray Diffraction and X-ray Absorption Spectroscopy. *Am. Mineral.* 2007, 92, 1875−1880.

(40) Lo, A. Y. H.; Sudarsan, V.; Sivakumar, S.; van Veggel, F.; Schurko, R. W. Multinuclear Solid-state NMR Spectroscopy of Doped Lanthanum Fluoride Nanoparticles. *J. Am. Chem. Soc.* 2007, 129, 4687−4700.

(41) Sebastian, C. P.; Zhang, L.; Fehse, C.; Hoffmann, R. D.; Eckert, H.; Pottgen, R. New Stannide ScAgSn: Determination of the Superstructure via Two-dimensional Sc-45 Solid State NMR. *Inorg. Chem.* 2007, 46, 771−779.

(42) Jayasundera, A. C. A.; Finch, A. A.; Wormald, P.; Lightfoot, P. Solvothermal Synthesis and Luminescent Properties of Two Organically Templated Chain-Structure Fluorides, $[C_4H_{14}N_2][MF_5]$ (M = In, Sc). *Chem. Mater.* 2008, 20, 6810−6815.

(43) Mohr, D.; de Camargo, A. S. S.; Schneider, J. F.; Queiroz, T. B.; Eckert, H.; Botero, E. R.; Garcia, D.; Eiras, J. A. Solid State NMR as a New Approach for the Structural Characterization of Rare-earth

Doped Lead Lanthanum Zirconate Titanate Laser Ceramics. *Solid State Sci.* **2008**, *10*, 1401−1407.

(44) Huang, H.; Hsieh, C. H.; Kim, N.; Stebbins, J.; Pninz, F. Structure, Local Environment, and Ionic Conduction in Scandia Stabilized Zirconia. *Solid State Ionics* **2008**, *179*, 1442−1445.

(45) Kim, N.; Stebbins, J. F. $Sc_2(WO_4)_3$ and $Sc_2(MoO_4)_3$ and Their Solid Solutions: Sc-45, O-17, and Al-27 MAS NMR Results at Ambient and High Temperature. *Chem. Mater.* **2009**, *21*, 309−315.

(46) Balamurugan, S.; Rodewald, U. C.; Harmening, T.; van Wullen, L.; Mohr, D.; Eckert, H.; Pottgen, R. $Sc_2(MoO_4)_3$ and $Sc_2(WO_4)_3$: Halide Flux Growth of Single Crystals and Sc-45 Solid-state NMR. *Z. Naturforsch., B* **2010**, *65*, 13−17.

(47) Balamurugan, S.; Rodewald, U. C.; Harmening, T.; van Wullen, L.; Mohr, D.; Deters, H.; Eckert, H.; Pottgen, R. PbO/PbF_2 Flux Growth of $YScO_3$ and $LaScO_3$ Single Crystals - Structure and Solid-State NMR Spectroscopy. *Z. Naturforsch., B* **2010**, *65*, 1199−1205.

(48) Alba, M. D.; Chain, P.; Florian, P.; Massiot, D. ^{45}Sc Spectroscopy of Solids: Interpretation of Quadrupole Interaction Parameters and Chemical Shifts. *J. Phys. Chem. C* **2010**, *114*, 12125−12132.

(49) Buannic, L.; Blanc, F.; Hung, I.; Gan, Z. H.; Grey, C. P. Probing the Local Structures and Protonic Conduction Pathways in Scandium Substituted $BaZrO_3$ by Multinuclear Solid-state NMR Spectroscopy. *J. Mater. Chem.* **2010**, *20*, 6322−6332.

(50) Mowat, J. P. S.; Miller, S. R.; Slawin, A. M. Z.; Seymour, V. R.; Ashbrook, S. E.; Wright, P. A. Synthesis, Characterisation and Adsorption Properties of Microporous Scandium Carboxylates with Rigid and Flexible Frameworks. *Microporous Mesoporous Mater.* **2011**, *142*, 322−333.

(51) Pahari, B.; Iftekhar, S.; Jaworski, A.; Okhotnikov, K.; Jansson, K.; Stevensson, B.; Grins, J.; Eden, M. Composition-Property-Structure Correlations of Scandium Aluminosilicate Glasses Revealed by Multinuclear ^{45}Sc, ^{27}Al, and ^{29}Si Solid-State NMR. *J. Am. Ceram. Soc.* **2012**, *95*, 2545−2553.

(52) Johnston, K. E.; Mitchell, M. R.; Blanc, F.; Lightfoot, P.; Ashbrook, S. E. Structural Study of $La_{1−x}Y_xScO_3$, Combining Neutron Diffraction, Solid-State NMR, and First-Principles DFT Calculations. *J. Phys. Chem. C* **2013**, *117*, 2252−2265.

(53) Merkens, C.; Pecher, O.; Steuber, F.; Eisenhut, S.; Gorne, A.; Haarmann, F.; Englert, U. Crystal-to-Crystal Transformations in a Seven-Coordinated Scandium Complex. *Z. Anorg. Allg. Chem.* **2013**, *639*, 340−346.

(54) Arnold, P. L.; Marr, I. A.; Zlatogorsky, S.; Bellabarba, R.; Tooze, R. P. Activation of Carbon Dioxide and Carbon Disulfide by a Scandium N-heterocyclic Carbene Complex. *Dalton Trans.* **2014**, *43*, 34−37.

(55) Fuchs, R.; Strahle, J. Crystal-Structure of $Sc(CH_3COO)_3$, a Metal(III) Acetate with a Chain Structure. *Z. Naturforsch., B* **1984**, *39*, 1662−1663.

(56) Bodart, P. R.; Amoureux, J. P.; Dumazy, Y.; Lefort, R. Theoretical and Experimental Study of Quadrupolar Echoes for Half-integer Spins in Static Solid-state NMR. *Mol. Phys.* **2000**, *98*, 1545−1551.

(57) Iuga, D.; Schafer, H.; Verhagen, R.; Kentgens, A. P. M. Population and Coherence Transfer Induced by Double Frequency Sweeps in Half-integer Quadrupolar Spin Systems. *J. Magn. Reson.* **2000**, *147*, 192−209.

(58) Kentgens, A. P. M.; Verhagen, R. Advantages of Double Frequency Sweeps in Static, MAS and MQMAS NMR of Spin I = 3/2 Nuclei. *Chem. Phys. Lett.* **1999**, *300*, 435−443.

(59) Eichele, K.; Wasylishen, R. E. *WSolids1: Solid-State NMR Spectrum Simulation*, V1.17.28 ed.; 2001.

(60) Rose, M. E. *Elementary Theory of Angular Momentum*; Wiley: New York, 1957.

(61) Peersen, O.; Wu, X.; Kustanovich, I.; Smith, S.; Variable-Amplitude Cross-Polarization, M. A. S. NMR. *J. Magn. Reson., Ser. A* **1993**, *104*, 334−339.

(62) Bennett, A. E.; Rienstra, C. M.; Auger, M.; Lakshmi, K. V.; Griffin, R. G. Heteronuclear Decoupling in Rotating Solids. *J. Chem. Phys.* **1995**, *103*, 6951.

(63) Kraus, W.; Nolze, G. *PowderCell for Windows*, V2.3; Federal Institute for Materials Research and Testing: Berlin, Germany, 2000.

(64) Abbasi, A.; Lindqvist-Reis, P.; Eriksson, L.; Sandstrom, D.; Lidin, S.; Persson, I.; Sandstrom, M. Highly Hydrated Cations: Deficiency, Mobility, and Coordination of Water in Crystalline Nonahydrated Scandium(III), Yttrium(III), and Lanthanoid(III) Trifluoromethanesulfonates. *Chem.—Eur. J.* **2005**, *11*, 4065−4077.

(65) Lindqvist-Reis, P.; Persson, I.; Sandstrom, M. The Hydration of the Scandium(III) Ion in Aqueous Solution and Crystalline Hydrates Studied by XAFS Spectroscopy, Large-angle X-ray Scattering and Crystallography. *Dalton Trans.* **2006**, 3868−3878.

(66) Rudolph, W. W.; Pye, C. C. Aqueous Solution Chemistry of Scandium(III) Studied by Raman Spectroscopy and ab initio Molecular Orbital Calculations. *J. Solution Chem.* **2000**, *29*, 955−986.

(67) Rudolph, W. W.; Pye, C. C. Raman Spectroscopic Measurements of Scandium(III) Hydration in Aqueous Perchlorate Solution and ab initio Molecular Orbital Studies of Scandium(III) Water Clusters: Does Sc(III) Occur as a Hexaaqua Complex? *J. Phys. Chem. A* **2000**, *104*, 1627−1639.

(68) Rotzinger, F. P. Mechanism of Water Exchange for the Di- and Trivalent Metal Hexaaqua Ions of the First Transition Series. *J. Am. Chem. Soc.* **1997**, *119*, 5230−5238.

(69) Akesson, R.; Pettersson, L. G. M.; Sandstrom, M.; Wahlgren, U. Ligand-Field Effects in the Hydrated Divalent and Trivalent Metal-Ions of the First and 2nd Transition Periods. *J. Am. Chem. Soc.* **1994**, *116*, 8691−8704.

(70) Gottlieb, H. E.; Kotlyar, V.; Nudelman, A. NMR Chemical Shifts of Common Laboratory Solvents as Trace Impurities. *J. Org. Chem.* **1997**, *62*, 7513−7514.

(71) van Eck, E. R. H.; Janssen, R.; Maas, W. E. J. R.; Veeman, W. S. A Novel Application of Nuclear Spin-echo Double-resonance to Aluminophosphates and Aluminosilicates. *Chem. Phys. Lett.* **1990**, *174*, 428.

(72) Grey, C.; Vega, A. Determination of the Quadrupole Coupling Constant of the Invisible Aluminum Spins in Zeolite HY with $^1H/^{27}Al$ TRAPDOR NMR. *J. Am. Chem. Soc.* **1995**, *117*, 8232−8242.

(73) Amoureux, J. P.; Trebosc, J.; Delevoye, L.; Lafon, O.; Hu, B.; Wang, Q. Correlation NMR Spectroscopy Involving Quadrupolar Nuclei. *Solid State Nucl. Magn. Reson.* **2009**, *35*, 12−18.

(74) The hydrated species $Sc(OTf)_3 \cdot 8H_2O$ and $Sc(OTf)_3 \cdot xH_2O$ also possess ^1H chemical shifts of ca. 7 ppm (Supporting Information Figure S2); however, the ^{19}F spectra clearly indicate that only anhydrous $Sc(OTf)_3$ is present in the material. Therefore, the observed proton signal in the $^{19}F–^1H$ CPMAS spectrum must correspond to the aromatic protons.

(75) Munoz-Espi, R.; Jeschke, G.; Lieberwirth, I.; Gomez, C. M.; Wegner, G. ZnO-Latex Hybrids Obtained by Polymer-controlled Crystallization: A Spectroscopic Investigation. *J. Phys. Chem. B* **2007**, *111*, 697−707.

(76) Verploegen, E.; Dworken, B. T.; Faught, M.; Kamperman, M.; Zhang, Y. M.; Wiesner, U. Tuning Mechanical Properties of Block Copolymer/Aluminosilicate Hybrid materials. *Macromol. Rapid Commun.* **2007**, *28*, 572−578.

(77) Fahmi, A.; Pietsch, T.; Mendoza, C.; Cheval, N. Functional Hybrid Materials. *Mater. Today* **2009**, *12*, 44−50.

(78) Li, Z. H.; Sai, H.; Warren, S. C.; Kamperman, M.; Arora, H.; Gruner, S. M.; Wiesner, U. Metal Nanoparticle-Block Copolymer Composite Assembly and Disassembly. *Chem. Mater.* **2009**, *21*, 5578−5584.

(79) Bang, J.; Jeong, U.; Ryu, D. Y.; Russell, T. P.; Hawker, C. J. Block Copolymer Nanolithography: Translation of Molecular Level Control to Nanoscale Patterns. *Adv. Mater.* **2009**, *21*, 4769−4792.

(80) Kim, H. C.; Park, S. M.; Hinsberg, W. D. Block Copolymer Based Nanostructures: Materials, Processes, and Applications to Electronics. *Chem. Rev.* **2010**, *110*, 146−177.

(81) Tretinnikov, O. N. Hydrophilic (Hydrogen-Bonding) Polystyrene Surface by Substrate-induced Surface Segregation of Benzene groups. *Langmuir* **2000**, *16*, 2751−2755.

(82) Bistac, S.; Schmitt, M.; Ghorbal, A.; Gnecco, E.; Meyer, E. Nano-scale Friction of Polystyrene in Air and in Vacuum. *Polymer* **2008**, *49*, 3780−3784.

(83) Takeuchi, M.; Akiyama, R.; Kobayashi, S. Polymer-micelle Incarcerated Scandium as a Polymer-supported Catalyst for High-throughput Organic Synthesis. *J. Am. Chem. Soc.* **2005**, *127*, 13096−13097.

(84) Mantri, K.; Komura, K.; Kubota, Y.; Sugi, Y. Friedel-Crafts Alkylation of Aromatics with Benzyl Alcohols Catalyzed by Rare Earth Metal Triflates Supported on MCM-41 Mesoporous Silica. *J. Mol. Catal. A: Chem.* **2005**, *236*, 168−175.

(85) Choudary, B. M.; Roy, M.; Roy, S.; Kantam, M. L.; Sreedhar, B.; Kumar, K. V. Preparation, Characterization and Catalytic Properties of Polyaniline-supported Metal Complexes. *Adv. Synth. Catal.* **2006**, *348*, 1734−1742.

(86) Annis, D. A.; Jacobsen, E. N. Polymer-supported Chiral Co(salen) Complexes: Synthetic Applications and Mechanistic Investigations in the Hydrolytic Kinetic Resolution of Terminal Epoxides. *J. Am. Chem. Soc.* **1999**, *121*, 4147−4154.

(87) Kobayashi, S.; Endo, M.; Nagayama, S. Catalytic Asymmetric Dihydroxylation of Olefins Using a Recoverable and Reusable Polymer-supported Osmium Catalyst. *J. Am. Chem. Soc.* **1999**, *121*, 11229−11230.

(88) Nagayama, S.; Kobayashi, S. A Novel Polymer-supported Scandium Catalyst Which Shows High Activity in Water. *Angew. Chem., Int. Ed.* **2000**, *39*, 567−569.

(89) Saladino, R.; Neri, V.; Pelliccia, A. R.; Caminiti, R.; Sadun, C. Preparation and Structural Characterization of Polymer-supported Methylrhenium Trioxide Systems as Efficient and Selective catalysts for the Epoxidation of Olefins. *J. Org. Chem.* **2002**, *67*, 1323−1332.

(90) Gibson, S. E.; Swamy, V. M. Microencapsulation of a Metathesis Catalyst. *Adv. Synth. Catal.* **2002**, *344*, 619−621.

(91) Lattanzi, A.; Leadbeater, N. E. Microencapsulated $VO(acac)_2$: Preparation and Use in Allylic Alcohol Epoxidation. *Org. Lett.* **2002**, *4*, 1519−1521.

(92) Srirattnai, K.; Damronglerd, S.; Omi, S.; Roengsumran, S.; Petsom, A.; Ma, G. H. Encapsulated $AlCl_3$: A Convenient Catalyst for the Alkylation of Benzene with Dodecene. *Tetrahedron Lett.* **2002**, *43*, 4555−4557.

(93) He, H. S.; Yan, J. J.; Shen, R. X.; Zhuo, S. J.; Toy, P. H. Non-cross-linked Polystyrene-supported Triphenylphosphine-microencapsulated Palladium: An Efficient and Recyclable Catalyst for Suzuki-Miyaura Reactions. *Synlett* **2006**, 563−566.

(94) Liu, G. Y.; Wu, B.; Zhang, J. Z.; Wang, X. L.; Shao, M. B.; Wang, J. H. Controlled Reversible Immobilization of Ru Carbene on Single-Walled Carbon Nanotubes: A New Strategy for Green Catalytic Systems Based on a Solvent Effect on pi-pi Interaction. *Inorg. Chem.* **2009**, *48*, 2383−2390.

(95) Rahmatpour, A.; Aalaie, J. One-Pot Synthesis of N-Substituted Pyrroles Catalyzed by Polystyrene-Supported Aluminum Chloride as a Reusable Heterogeneous Lewis Acid Catalyst. *Heteroat. Chem.* **2011**, *22*, 85−90.

(96) Perrier, A.; Keller, M.; Caminade, A. M.; Majoral, J. P.; Ouali, A. Efficient and Recyclable Rare Earth-based Catalysts for Friedel-Crafts Acylations Under Microwave Heating: Dendrimers Show the Way. *Green Chem.* **2013**, *15*, 2075−2080.

(97) Zhang, F.; Liang, C.; Chen, M. Z.; Guo, H. B.; Jiang, H. Y.; Li, H. X. An Extremely Stable and Highly Active Periodic Mesoporous Lewis Acid Catalyst in Water-medium Mukaiyama-aldol Reaction. *Green Chem.* **2013**, *15*, 2865−2871.